AD-A124 663 TRANSIENT HEAT-TRANSFER MEASUREMENT TECHNIQUE IN WIND TUNNEL AND DATA ANA..(U) AIR FORCE INST OF TECH WRIGHT-PATTERSON AFB OH SCHOOL OF ENGI.. Y K WOO 1/1

UNCLASSIFIED DEC 82 AFIT/GAE/AA/82D-34 F/G 14/2 NL

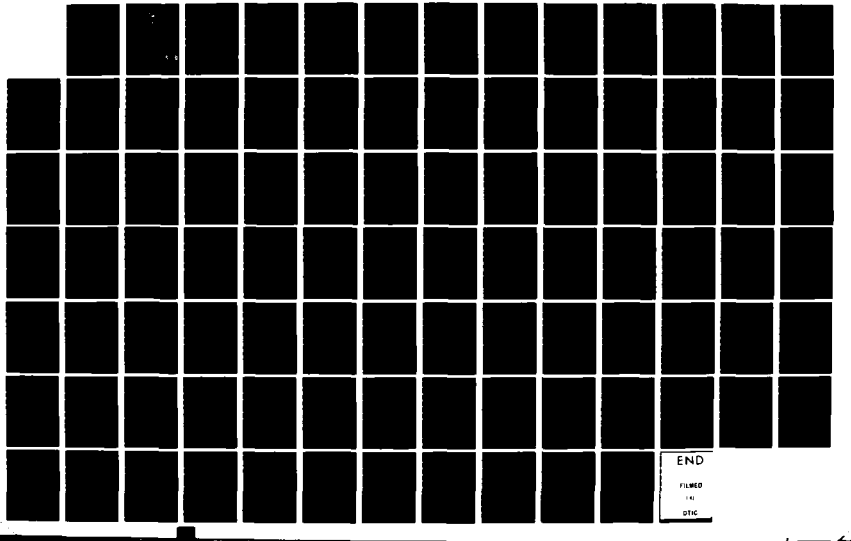

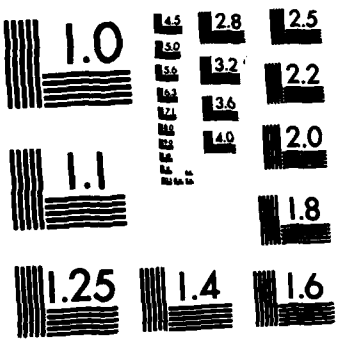

TRANSIENT HEAT-TRANSFER MEASUREMENT TECHNIQUE IN WIND TUNNEL AND DATA ANALYSIS TECHNIQUE USING SYSTEM IDENTIFICATION THEORY

ESIS

AFIT/GAE/AA/82D-34

Yuk K. Woo
2nd Lt USAF

DEPARTMENT OF THE AIR FORCE
AIR UNIVERSITY (ATC)
AIR FORCE INSTITUTE OF TECHNOLOGY

Wright-Patterson Air Force Base, Ohio

TRANSIENT HEAT-TRANSFER MEASUREMENT TECHNIQUE IN WIND TUNNEL AND DATA ANALYSIS TECHNIQUE USING SYSTEM IDENTIFICATION THEORY

THESIS

AFIT/GAE/AA/82D-34

Yuk K. Woo
2nd Lt USAF

AFIT/GAE/AA/82D-34

TRANSIENT HEAT-TRANSFER MEASUREMENT TECHNIQUE IN WIND TUNNEL AND DATA ANALYSIS TECHNIQUE USING SYSTEM IDENTIFICATION THEORY

THESIS

Presented to the Faculty of the School of Engineering

of the Air Force Institute of Technology

Air University

in Partial Fulfillment of the

Requirements for the Degree of

Master of Science

by

Yuk K. Woo, B.S.

2nd Lt USAF

Graduate Aeronautical Engineering

December 1982

Preface

There are two objectives I want to bring out in this thesis. First, the main objective is to verify the feasibility of the new flight testing technique for the Space Shuttle Orbiter in a controlled environment. This is discussed fully in the last section of this report. Secondly, I attempt to summarize the data reduction method used in the rest of the report. The mathematical formulation may be hard to follow, especially the stochastic estimation section of this report. I recommend that the reader refer to Maybeck's books on the subject. I found it easier to read than most other reference material that I have come across. Hopefully, this will help as far as this section is concerned, and the rest is straightforward.

I wish to express my gratitude to the Air Force Wright Aeronautical Laboratories (AFWAL) for making available the wind tunnel data and also the descriptions of the wind tunnel test articles. Without the material provided, I would not have been able to put together this thesis. I am indebted to my thesis advisor, Capt James K. Hodge of the Department of Aeronautics and Astronautics at the Air Force Institute of Technology (AFIT). His helpful suggestions and his constant encouragement and understanding has made all this possible. I also would like to thank Dr. Will Hankey of the AFWAL and Capt David R. Audley of the Mathematics Department at AFIT for the input and suggestions that kept me on the right track throughout this thesis. Last, I would like to thank Mrs. Cindy McDonald for her effort in typing my thesis.

November 1982

Yul K. Woo

Contents

Contents

List of Figures

List of Figures

List of Tables

Nomenclature

A	generic matrix of the state space model (n x n)
a_{ij}	element of the A matrix
$\underline{B}$	deterministic forcing function (n dimension)
b_i	element of the $\underline{B}$ vector
C_i	material specific heat
C_p	specific heat of air
D_i	coefficient of the sensitivity equations
$E\{\cdot\}$	stochastic expectation
$F(t_i)$	covariance matrix
$f(\alpha)$	a function of angle of attack
H	measurement matrix
h	heat transfer film coefficient
h_{ref}	reference heat transfer film coefficient
$\bar{h}$	non-dimensionless heat transfer film coefficient
$\bar{h}_o$	non-dimensionless zero intercept
$\bar{h}_\alpha$	non-dimensional heating derivative with respect to the angle of attack
I	identity matrix
$J[\cdot]$	conditional information matrix
K_i	material thermal conductivity
$K(t_i)$	Kalman gain at time t_i
$L[\cdot]$	likelihood function
M_i	coefficient of the sensitivity equations
n	number of node points
$P(t)$	covariance matrix

Nomenclature

P_r	Prandtl number
$Q(t)$	m x m white noise strength matrix
q	force convective heating rate
$\overline{R}$	recovery factor
R	white noise strength matrix
S_{θ_K}	sensitivity
U_o	total temperature
u	input
U_i	temperature at each node point
$\dot{U}_i$	time rate of change of temperature at each node
$\underline{\dot{U}}(t)$	time rate of change of temperature state vector
U_∞	free space temperature or radiation sink temperature
$\underline{\hat{U}}$	mean vector
$\underline{\hat{U}}_*(t_i)$	best temperature estimates using currently available $\underline{U}_*(t_i)$
$\underline{U}^*(t_i)$	optimal temperature estimates at time t_i
$\underline{V}(t_i)$	white noise incorporated with the measurement
V	freestream velocity
$\underline{W}(t)$	white noise incorporated with the model
X	distance from the leading edge
$\underline{Y}(t_i)$	thermocouple measurements at discrete-time sample
y_i	set of realization of the measurements
$\underline{y}_i$	dummy variable incorporated with the measurement data
z	output

Nomenclature

α	angle of attack
α_o	reference angle of attack
ρ	freestream density
ρ_i	material density
μ	viscosity
Θ	set of unknown parameters
θ	dummy variable incorporated with the unknown parameters
Θ^*	optimal parameter estimates
$\hat{\theta}_*$	a priori parameter estimates
$\hat{\theta}^*$	a posterior parameter estimates
$\phi(t-t_o)$	state transition matrix
ξ	dummy variable incorporated with temperature profile
∇_ξ	gradients with respect to ξ
∇_θ	gradients with respect to θ
$\phi_K K_B$	thermal conductivity factor
$\delta(t-\tau)$	Dirac delta function
σ	Stefan-Boltzmann constant
ϵ	thermal emissivity
Δx_i	the distance between nodes
+	a posterior update
-	a priori propagation

Abstract

A transient maneuver testing technique has been developed by the Air Force Flight Test Center (AFFTC) for aerothermodynamic evaluation of the Space Shuttle Orbiter Thermal Protection System (TPS) during reentry. The objectives are to determine the feasibility of the testing technique and the feasibility of using the transient maneuver technique for wind tunnel heat transfer measurements. The transient maneuver technique can enhance the capability of wind tunnel testing by reducing the overall required testing time, and in turn lower the cost of testing significantly.

Wind tunnel data were obtained using the TPS materials of the Orbiter as wind tunnel test articles. Transient and steady state deflection angle data were obtained and analyzed. The thermocouple measurements along with the wind tunnel conditions were used as inputs to a heat estimation computer program. The program named "HEATEST" was developed by AFFTC and used system identification theory. The results of the estimates were compared with the available thin skin data and also with the Eckert flat plate theory.

The principal finding indicates the heating estimates are significantly lower for the TPS test articles than the thin skin test article and Eckert theory. The discrepancy is believed to be caused mainly by the non-isothermal wall effect. Finally, the transient maneuver testing technique has been proven since the transient maneuvers agree well with the steady state results.

I. Introduction

Background

Today's space transportation system, the Space Shuttle Orbiter, is very versatile. One unique feature about the Shuttle is its reusable Thermal Protection System (TPS), which consists primarily of low density ceramic tiles. (Ref. 13) For example, the TPS found on the lower surface of the Orbiter are High-Temperature, Reusable Surface Insulation (HRSI) tiles made of a special kind of low density ceramic. Flexible Reusable Surface Insulation (FRSI) made of coated Nomex felt can be found on the upper surface where temperatures are not as high. Although the TPS has been evaluated by ground testing in a controlled environment, it was not tested in a real flight environment before the first flight in April, 1981. For safety reasons, the mission of the Space Shuttle Orbiter has been limited to a narrow range of operations. Therefore, a primary goal is to expand the operational envelope of the Space Shuttle.

National Aeronautics and Space Administration (NASA) initiated a flight test program to assess the capability of the Space Shuttle Orbiter. The first several flights were initially designed for flight test purposes. The first flight test demonstrated the safe operation of the Space Shuttle. The subsequent flights are carefully designed to gradually expand the operational envelope of the Space Shuttle Orbiter. Although the assessment program consists of ascent, orbital and reentry phases of operations, the main emphasis in this report will be on the reentry phase. (Ref. 6)

With the baseline assessment program in mind, a new flight test technique has been developed by the Air Force Flight Test Center (AFFTC) to aid in the evaluation of the reentry aerothermodynamic environment of the Orbiter. The new assessment technique consists of three basic steps. First, wind tunnel data and a flight simulator were utilized for preliminary flight test evaluation and planning. Secondly, a new data acquisition technique was developed which combines the use of thermocouples and a transient maneuver testing technique to obtain flight data. Lastly, a flight data reduction technique was developed which utilizes thermocouple measurements to estimate the aerothermodynamic heating of the Orbiter. The overall results will ensure a rapid but safe envelope expansion of the Space Shuttle Orbiter. (Ref. 2,10,11)

Flight Test Technique

Mathematical models were developed by AFFTC for the flight simulator at AFFTC. (Ref. 10) Mathematical models were developed for seven locations on the Orbiter. These locations are ctitical for overall mission evaluation. They are assumed independent from one another. In addition, results at one point are not extrapolated to any other point on the Orbiter by these models. The locations are shown in Figure 1. Thermocouples were imbedded in the TPS at numerous locations on the Orbiter. (Ref. 17) The models will be used on the flight simulator to simulate the aerothermodynamic environment at each one of these locations or at any other locations which may be critical. The results from the simulator can then be used for evaluation and planning of the real flight test maneuvers. In addition, the mathematical models will be used for flight data analysis purposes. Similar models were used in wind tunnel data analysis.

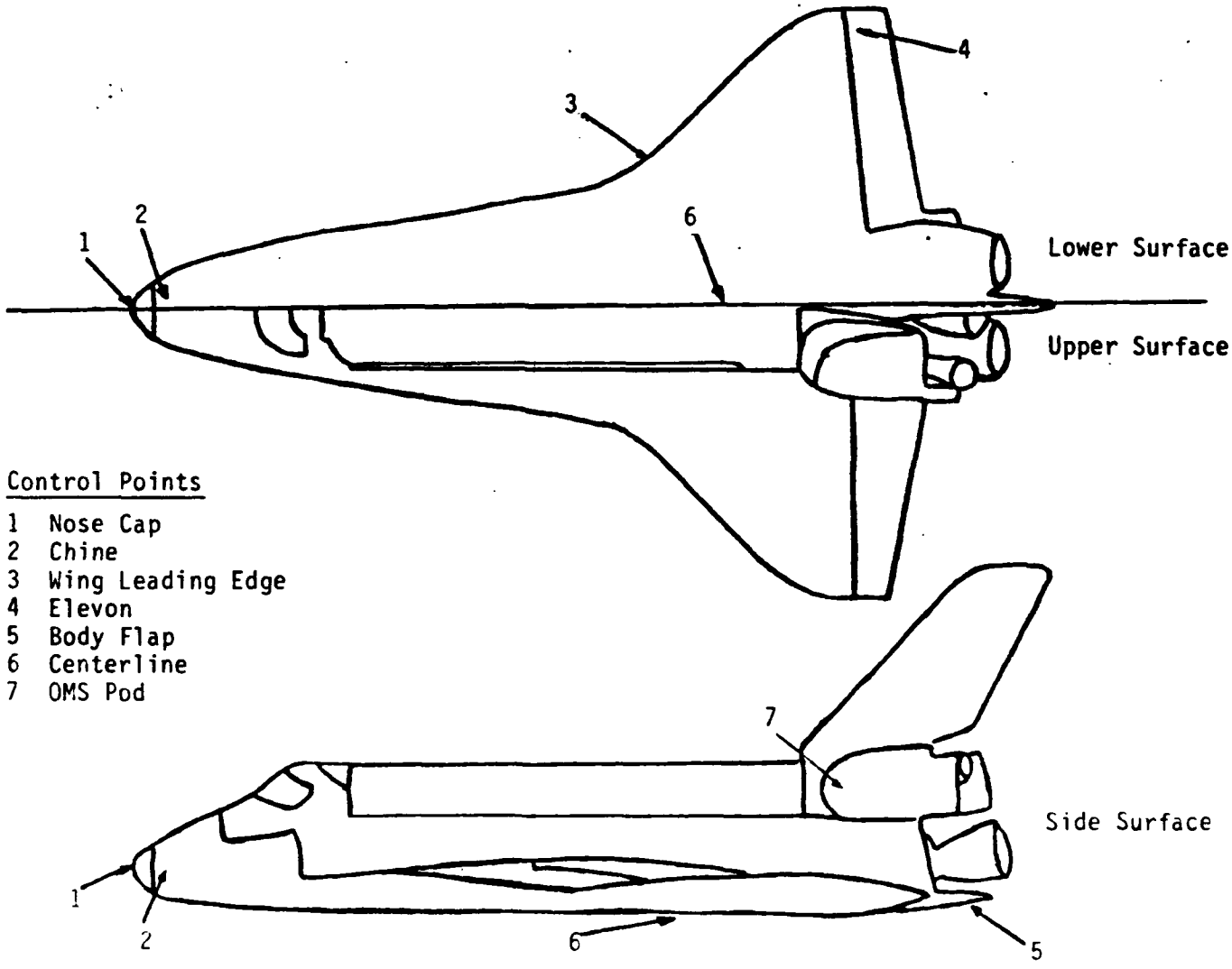

Figure 1 Space Shuttle Control Point Locations

Transient flight test maneuvers have been and will be performed during the Orbiter test flights, and flight test data will be obtained under these conditions. One example is the pushover-pullup maneuver performed during the Orbiter's second test flight. (Ref. 10) One requirement is that the duration of the transient maneuvers should be short enough to not affect the overall trajectory of the mission. Moreover, the maneuvers are being gradually expanded on subsequent flights.

The thermocouple data from the flight test are being analyzed, and a digital computer is suited for this purpose. A heat-estimate computer program called "HEATEST" has been developed by the AFFTC. The "HEATEST" computer program utilizes the state estimation and system identification theory to estimate the aerothermodynamic parameters.

The system identification theory in this case simply uses the available information given about the input and the output of the process and uses this information to estimate the parameters of interest in the process. For example, in Figure 2, the u and z is the input and the output of the system which can be used to characterize the complete process in the box.

Figure 2. A Simple Control Input/Output System Model

The data analysis technique consisted of a state predictor-corrector and a parameter estimation scheme. The predictor-corrector scheme requires a stochastic process model which was developed for the simulator

to propagate or predict the temperatures and use the Kalman estimator or filter to update or correct the temperature of the model. (Ref. 12, 14)

The parameters are estimated by maximizing a likelihood function. (Ref. 1, 2, 8, 14, 16) The results will be a best estimate of the parameters.

At last, the flight testing technique combines the wind tunnel and the flight test results to generate an enriched simulator data base for understanding the heating behavior of the Orbiter during reentry.

Purpose

This flight testing technique can also be used in a wind tunnel. The transient maneuver testing technique can reduce the testing time in the wind tunnel significantly. This will, in a way, enhance the capability of wind tunnel testing. The purpose of this thesis is to use the data reduction technique which was developed for the flight data analysis, and the wind tunnel experimental data obtained by the Air Force Wright Aeronautical Laboratories (AFWAL) to verify the feasibility of the transient maneuvers in the wind tunnel. Initially, the wind tunnel test was conducted to verify the flight testing technique before the first flight test maneuvers were committed. The reason was that the wind tunnel data could be obtained in a controlled environment. For example, wind tunnel data will not have real gas effects, limited data sampling rate, eight-bit noise, and the time skews experienced in the flight measurements. For this reason, the results of the wind tunnel tests could answer some of the questions about the flight techniques that were not available before. Based on these, the flight testing technique can then be improved in the future.

Overview

In the following sections, the mathematical models and the stochastic modelling process will be presented. A state estimator and a parameter estimation technique will be discussed in full detail. Then, the wind tunnel results will be discussed.

II. Mathematical Modelling Process

Introduction

Mathematical models were developed for a flight simulator and also used for flight data analysis. In this case, the models were used for wind tunnel data analysis. Models for the aerodynamic forced convective heating at the surface of the TPS and the thermal conduction through the tiles will be discussed. These two models will be treated separately at the beginning of the modelling process. In the end, a complete state space model of the process will be discussed.

Heating Model

The aerodynamic heating rate at the surface was modelled for two TPS test articles in the wind tunnel. The convective heat-transfer can be written as

$$q = \bar{h}(\bar{R}U_0 - U_1) \qquad 2.1a$$

or in terms of the heat-transfer film coefficient,

$$h = q / (\bar{R}U_0 - U_1) \qquad 2.1b$$

where U_0 is the stagnation temperature, U_1 is the surface temperature, and $\bar{R}$ is the recovery factor which is assumed to be 0.9. The heating models were assumed to be functions of the freestream conditions in the wind tunnel test section. In addition, the aerodynamic heating rate was assumed to be linear in deflection angle. This is not a bad assumption based on previous experiments and also from Eckert flat plate theory. Therefore, the linearized heating model can be formulated as follows:

$$\bar{h} = \frac{h}{h_{ref}} = f(\alpha) = \bar{h}_0 + \bar{h}_\alpha(\alpha - \alpha_0) \qquad 2.2a$$

where $\bar{h}$ is a dimensionless heat-transfer film coefficient which was non-dimensionalized by dividing a reference heat-transfer film coefficient. (Ref. 9,10,11,17)

$$h_{ref} = \frac{.332}{Pr^{2/3}}\sqrt{\frac{\rho V \mu}{x}}\left(\frac{C_p}{778.3}\right) \qquad 2.2b$$

h_{ref} is based on Eckert flat plate theory for laminar flow with zero deflection angle. (Ref. 7) Laminar flow is appropriate for the wind tunnel test which was conducted, but for the flight data analysis, turbulent flow might be used.

In equation 2.1, $\bar{h}_\alpha$ is the heating derivative with respect to the angle of attack α. $\bar{h}_0$ is the zero intercept at the reference value α_0.

The mathematical model will be used at the boundary or the surface condition for the development of the thermal model. Furthermore, the heating derivative and the zero intercept are the primary unknown to be estimated.

Thermal Model

A one-dimensional conduction model was assumed. (Ref. 10,11) The one-dimensional assumption was suitable for two reasons. First, conduction in the Space Shuttle TPS is very low, and the duration of the test maneuvers is short enough, so that the lateral conduction would be small. But if the lateral conduction became necessary in the calculation, an appropriate scaling factor will scale the thickness of the test article according to the amount of conduction generated in the lateral direction. (Ref. 10) Second, stochastic estimation was used in conjunction with the measured data from the real system to update

the estimated values. Therefore, the error generated by the assumption will be eliminated.

A cross-section of the thermal model is shown in Figure 3. For implementation on a digital computer, n-discrete node points were established to approximate the temperature profile in the model. There are four node points near boundary locations, and the rest are distributed in the Reusable Surface Insulation (RSI) tile. An energy/heat balance was used to formulate the following "n" heat transfer equations

$$C_A\rho_A\Delta X_A\dot{U}_1 = -2(K_A/\Delta X_A)U_1 + 2(K_A/\Delta X_A)U_2 - 2\sigma\varepsilon(U_1^4-U_\infty^4) + 2f(\alpha)h_{ref} \quad 2.3a$$

$$(C_A\rho_A\Delta X_A + C_B\rho_B\Delta X_2)\dot{U}_2 = 2(K_A/\Delta X_A)U_1 - 2(K_A/\Delta X_A + K_B/\Delta X_2)U_2 + 2(K_B/\Delta X_2)U_3 \quad 2.3b$$

$$C_B\rho_B(\Delta X_{i-1} + \Delta X_i)\dot{U}_i = 2(K_B/\Delta X_{i-1})U_{i-1} - 2(K_B/\Delta X_{i-1} + K_B/\Delta X_i)U_i + 2(K_B/\Delta X_{i+1})U_{i+1} \quad 2.3c$$

$$(C_B\rho_B\Delta X_{L-3} + C_C\rho_C\Delta X_C)\dot{U}_{L-2} = 2(K_B/\Delta X_{L-3})U_{L-3} - 2(K_B/\Delta X_{L-3} + K_C/\Delta X_C)U_{L-2} + 2(K_C/\Delta X_C)U_{L-1} \quad 2.3d$$

$$(C_C\rho_C\Delta X_C + C_D\rho_D\Delta X_D)\dot{U}_{L-1} = 2(K_C/\Delta X_C)U_{L-2} - 2(K_C/\Delta X_C + K_D/\Delta X_D)U_{L-1} + 2(K_D/\Delta X_D)U_L \quad 2.3e$$

$$C_D\rho_D\Delta X_D\dot{U}_L = 2(K_D/\Delta X_D)U_{L-1} - 2(K_D/\Delta X_D)U_L \quad 2.3f$$

where C_j, ρ_j and K_j, $j = A,B,C,D$, are the material properties. The material specific heat C_j and the thermal conductivity K_j are a function of the temperature at each node point, and the thermal conductivity is also a function of the local pressure in the tile. Therefore, K_j is approximated by the average temperature between nodes, and C_j is approximated at each node. U_i is the temperature at each node, and "." represents a time rate of change of temperature. Last, ΔX_i is the distance between nodes.

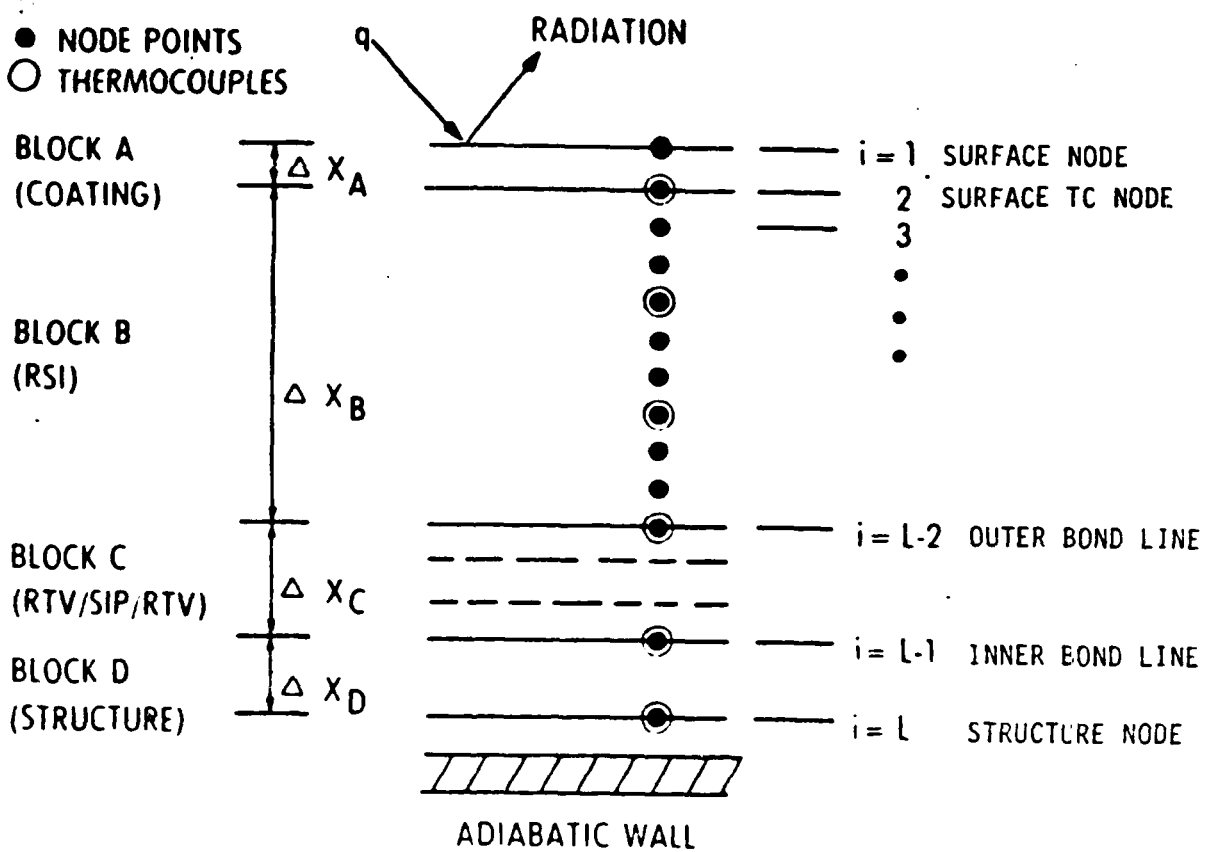

Figure 3 A Cross-Section of the TPS Thermal Model

The primary unknowns are mostly in Equation 3.2a, the surface boundary condition. The unknowns are the thermal emissivity ϵ, the aerodynamic heating rate $f(\alpha)$, and the coating thickness ΔX_A. For example, the emissivity can be as low as .75 and as high as .92. The thermal conductivity K_j was originally assumed to be "a priori" known parameter, but since the thermal conductivity depended on the pressure inside the TPS tile, and the pressure sensor in the TPS tile might not be able to measure the pressure correctly, the thermal conductivity is also treated as an unknown. The specific heat C_j and the density ρ_j are assumed to be a priori known based on the design specification.

Complete State Space Models with Stochastic Process

In order to determine the unknown parameters, system identification theory was used. One requirement is to introduce a stochastic modelling process. The model's uncertainty is associated with the approximation about the real process. The n-differential equations which were developed earlier can be arranged in a more convenient state space format. One reason for establishing a linear state space model is that a solution of the state can be easily found.

The radiation term in the boundary equation is highly nonlinear. In order to set up a linear state space form, the fourth order term $U_1^4(t_n)$ is approximated by (Ref. 3, 18)

$$U_1^4(t_n) \approx 4(U_1(t_{n-1}))^3 U_1(t_n) - 3(U_1(t_{n-1}))^4 \qquad 2.4$$

where $U_1(t_{n-1})$ is a known temperature which is propagated from the previous time. With this approximation, the n-differential equation

can be written in the form

$$\underline{U}(t) = A\underline{U}(t) + \underline{B} + \underline{W}(t) \qquad 2.5$$

where A is the n x n tridiagonal matrix of the material properties, and $\underline{B}$ is the n-dimensional vector of the deterministic inputs. (See Appendix A) $\underline{U}(t)$ is an n-dimensional state vector at time t. $\underline{W}(t)$ is an n-dimensional white Gaussian noise vector with statistics

$$E\{\underline{W}(t)\} = \underline{0} \qquad 2.6a$$

$$E\{\underline{W}(t)\underline{W}(\tau)^T\} = Q(t)\delta(t-\tau) \qquad 2.6b$$

where $E\{\cdot\}$ is the expectation, and Equation 2.6 represents a zero mean with covariance $Q(t)\delta(t-\tau)$. $Q(t)$ is an m x m matrix, and $\delta(t-\tau)$ is the Dirac delta function. The property of the Dirac delta function is simply zero everywhere except at $\tau=t$. (Ref. 2,5,12,14)

There are reasons why white Gaussian noise was used. White noise is uncorrelated in time, and has equal power in all frequencies. Because equal power in all frequencies means infinite power, white noise therefore can not exist in nature. There are two reasons why white noise can be used. First, a real system noise especially with a wideband noise usually can be approximated quite well with white noise. Second, the mathematics is greatly simplified with white noise.

A Gaussian process will ensure a "best" estimate since the mean, the maximum likelihood, and the median all coincide. In addition, only the first two moments are necessary to completely describe the statistics in the process. The first two moments are the mean and the covariance

of the process. Therefore, with a white Gaussian process, the complexity of the process can be considerably reduced. (Ref. 5,12,14)

Initial conditions are needed to completely characterize the state equations, but in many cases, initial conditions may not be known precisely. Therefore, the initial temperature $\underline{U}(t_0)$ are characterized by the statistics

$$E\{\underline{U}(t_0)\} = \hat{\underline{U}}_0 \qquad 2.7a$$

$$E\{[\underline{U}(t_0) - \hat{\underline{U}}_0][\underline{U}(t_0)-\hat{\underline{U}}_0]^T\} = P_0 \qquad 2.7b$$

where $\hat{\underline{U}}_0$ is the mean, and P_0 is a n x n covariance matrix. The initial noise is also assumed to be a Gaussian process. In addition, the best estimate of $\underline{U}(t_0)$ is assumed to be $\hat{\underline{U}}_0$.

To complete the modelling process, a measurement model is developed,

$$\underline{Y}(t_i) = H\underline{U}(t_i) + \underline{V}(t_i) \qquad 2.8$$

where $\underline{Y}(t_i)$ is k-vector measurements at a discrete time t_i. H is an k x n matrix which locates measurements relative to other nodes, and $\underline{V}(t_i)$ is a "stationary" white Gaussian process. The statistics of the k-vector is

$$E\{\underline{V}(t_i)\} = \underline{0} \qquad 2.9a$$

$$E\{\underline{V}(t_i)\underline{V}^T(t_j)\} = \begin{cases} R & t_i = t_j \\ 0 & t_i \neq t_j \end{cases} \qquad 2.9b$$

where R is a time invariant k x k matrix for stationary white Gaussian process. All sensors are assumed to be independent with each other.

In addition, processes $\underline{U}(t_o)$, $\underline{W}(t)$, and $\underline{V}(t_i)$ are also assumed to be independent with each other. At this point, a solution to the state space model can be found to be

$$\underline{U}(t) = \Phi(t - t_o)\underline{U}(t_o) + \int_{t_o}^{t} \Phi(t - \tau)\, \underline{B}(\tau)\, d\tau + \int_{t_o}^{t} \Phi(t - \tau)\underline{W}(\tau)d\tau \qquad 2.10$$

where $\Phi(t - t_o)$ is the state transition matrix,

$$\Phi(t - t_o) = \exp\,[A(t - t_o)] \qquad 2.11$$

In order to completely characterize the system, the first two moments are needed. The first moment is

$$\hat{\underline{U}}(t) = E\{\underline{U}(t)\} = \Phi(t - t_o)E\{\underline{U}(t_o)\} + E\left\{\int_{t_o}^{t} \Phi(t - \tau)\underline{B}(\tau)d\tau\right\} + E\left\{\int_{t_o}^{t} \Phi(t - \tau)\underline{W}(\tau)d\tau\right\} \qquad 2.12$$

Since $\underline{W}(\tau)$ has zero mean, and $\underline{B}(\tau)$ is not a stochastic process, equation (2.12) becomes

$$\hat{\underline{U}}(t) = \Phi(t - t_o)\hat{\underline{U}}(t_o) + \int_{t_o}^{t} \Phi(t - \tau)\, \underline{B}(\tau)d\tau \qquad 2.13$$

Similarily, the second moment is

$$P(t) = E\{(\underline{U}(t) - \hat{\underline{U}}(t))(\underline{U}(t) - \hat{\underline{U}}(t))^T\}$$

$$= \Phi(t - t_o)P(t_o)\,\Phi\,(t - t_o)^T + \int_{t_o}^{t} \Phi(t - \tau)Q(\tau)\Phi(t - \tau)^T d\tau \qquad .14$$

In summary, combining the measurement data and the statistical information, a best estimate of the state can be obtained. Since the measurement data is obtained from the real system, unknown parameters can be identified by solving the maximum likelihood criterion with an iteration scheme. The results will be a best possible estimate.

III. State and Parameter Estimating Technique

Kalman Estimator

The temperature profile can be estimated using a Kalman filter algorithm. This will be evident in the next section when solving for the maximum likelihood criterion. In order to estimate the temperature profile, the values of the unknown parameters have to be known, but for now, the parameters are assumed to be "a priori" known values in which

$$\underline{U}^*(t_i) = \hat{\underline{U}}(t_i^+) \Big| \theta = \Theta^* \tag{3.1}$$

where $\underline{U}^*(t_i)$ is assumed to be the "optimal" estimate, and $\hat{\underline{U}}(t_i^+)$ is the best estimate from the Kalman estimator using the a priori known values of the unknown parameters.

The estimator involved a predictor-corrector scheme. The temperature profile at time t_i is predicted by the heat and thermal models and the a priori information at time t_{i-1}. It is then updated by the measurement data at time t_i which is provided by the real system. The temperature profile is propagated with the same scheme through the entire time history. Therefore, the Kalman filter equations can be formulated as follows:

$$\hat{\underline{U}}(t_i^-) = \Phi(t_i - t_{i-1})\hat{\underline{U}}(t_{i-1}^+) + \int_{t_{i-1}}^{t_i} \Phi(t_i - \tau)\underline{B}(\tau)d\tau \tag{3.2}$$

$$P(t_i^-) = \Phi(t_i - t_{i-1})P(t_{i-1}^+)\Phi^T(t_i - t_{i-1})$$

$$+ \int_{t_{i-1}}^{t_i} \Phi(t_i - \tau)Q(\tau)\Phi(t_i - \tau)d\tau \tag{3.3}$$

where Equation 3.2 and 3.3 are the equivalent difference equation of Equation 2.13 and Equation 2.14. $\underline{\hat{U}}(t_i^-)$ and $P(t_i^-)$ are the predicted temperature profile and the covariance at time t_i using the updated values $\underline{\hat{U}}(t_{i-1}^+)$ and $P(t_{i-1}^+)$ from the previous time t_{i-1}.

The updated equations involve solving the conditional density function

$$f_{\underline{U}(t_i)/\underline{Y}(t_i)}(\underline{\xi}/\underline{\mathcal{Y}}_i) \qquad 3.4$$

conditioned on the entire measurement sequence $\underline{Y}(t_i)$ up to time t_i. The derivation can be found in Maybeck, and the final results can be written as (Ref. 2)

$$\underline{\hat{U}}(t_i^+) = \underline{\hat{U}}(t_i^-) + K(t_i)[\underline{\mathcal{Y}}_i - H\underline{\hat{U}}(t_i^-)] \qquad 3.5$$

$$P(t_i^+) = [I - K(t_i)H]P(t_i^-)[I - K(t_i)H]^T + K(t_i)P(t_i^-)K(t_i)^T \qquad 3.6$$

where the "Kalman gain"

$$K(t_i) = P(t_i^-)H^T[HP(t_i^-)H^T + R]^{-1} \qquad 3.7$$

$\underline{\hat{U}}(t_i^+)$ and $P(t_i^+)$ are the "a posteriori" estimates of the state and the covariance. Since the derivation of Equation 3.2 to Equation 3.6 have assumed the values of the unknown parameters are "apriori" known and which is not the case, a parameter estimation technique using system identification theory was introduced.

Maximum Likelihood Criterion

There are many methods which can be used for estimating parameters. A maximum likelihood technique was chosen in this case for several reasons. First, in certain cases, maximum likelihood technique had been shown to

have nice asymptotic properties. For example, with a nice probability density function, the mean, mode, and the median are usually very close together, and with these conditions, the maximum likelihood estimate will be very close to the "best" or the "optimal" value. Furthermore, the maximum likelihood method can be applied to a large variety of cases, and many other estimation techniques are just a special case of the maximum likelihood technique. (Ref. 1,14,16)

In order to establish the maximum likelihood criterion, the first step is to find a likelihood function that will be best suited for the estimation purpose. There are many likelihood functions which can be used, but one that has been found to be the best is (Ref. 2,14).

$$f_{\underline{U}(t_i),\underline{Y}(t_i)/\Theta}(\underline{\xi}, \underline{y}_i/\theta) \qquad 3.8$$

where Equation 3.8 is a joint probability density function of $\underline{U}(t_i)$ and $\underline{Y}(t_i)$ conditioned on Θ. (Ref. 2) $\underline{U}(t_i)$ is the temperature profile at time t_i. $\underline{Y}(t_i)$ is the measurements sequence up to time t_i, and Θ is a set of unknown parameters.

$$\underline{U}(t_i) = [U_1(t_i)U_2(t_i)\cdots Un(t_i)]^T$$

$$\underline{Y}(t_i) = [\underline{Y}(t_1)\underline{Y}(t_2) \cdots \underline{Y}(t_i)]^T$$

$$\Theta = [\Delta X_A, \phi_K K_B, \bar{h}_0, \bar{h}_\alpha]^T$$

i is a set of acquired measurement values to be used as data

$$\underline{y}_i = [y_1, y_2 \cdots y_s]$$

$\underline{\xi}$ and θ are the dummy variables corresponding to $\underline{U}(t_i)$ and Θ.

One way of maximizing the likelihood function is to take the gradients of Equation 3.8 with respect to the temperature state $\underline{\xi}$, and the unknown parameters θ. This is the same as finding an optimal set of $\underline{U}(t_i)$ and Θ at time t_i that is most likely to produce the measurements $\underline{Y}(t_i)$. The gradients of the likelihood function with respect to $\underline{\xi}$ and θ can be written as

$$\nabla_{\underline{\xi}} L[\underline{\xi},\theta; \underline{\mathbf{y}}_i] \Big|_{\substack{\underline{\xi} = \underline{U}(t_i)^* \\ \theta = \Theta^*}} = \underline{0}^T \qquad 3.9a$$

$$\nabla_{\theta} L[\underline{\xi},\theta; \underline{\mathbf{y}}_i] \Big|_{\substack{\underline{\xi} = \underline{U}(t_i)^* \\ \theta = \Theta^*}} = \underline{0}^T \qquad 3.9b$$

where $L[\underline{\xi},\theta; \underline{\mathbf{y}}_i]$ is the natural logarithm of Equation 3.8,

$$L[\underline{\xi},\theta; \underline{\mathbf{y}}_i] = \ln(f_{\underline{U}(t_i),\underline{Y}(t_i)/\Theta}\ (\underline{\xi}, \underline{\mathbf{y}}_i/\theta)) \qquad 3.10$$

A closed form solution for Equation 3.9 may not always be available. Therefore, an iterative algorithm was generated to solve the criterion presented in Equation 3.9. The iterative algorithm can be easily implemented on a digital computer.

Solution of the Maximum Likelihood Criterion

In order to satisfy the maximum likelihood criterion, first Bayes' rule is applied to Equation 3.8 repeatedly through the entire measurements sequence to obtain

$$f_{\underline{U}(t_i),\underline{Y}(t_i)} = f_{\underline{U}(t_i)/\underline{Y}(t_i)} \cdot f_{\underline{Y}(t_i)}$$

$$= f_{\underline{U}(t_i)/\underline{Y}(t_i)} \cdot f_{\underline{Y}(t_i)/\underline{Y}(t_{i-1})} \cdot f_{\underline{Y}(t_{i-1})}$$

$$\vdots$$

$$= f_{\underline{U}(t_i)/\underline{Y}(t_i)} \prod_{j=1}^{i} f_{\underline{Y}(t_j)/\underline{Y}(t_{j-1})} \qquad 3.11$$

where Θ has been suppressed to simplify the notations, and $f_{\underline{Y}(t_j)}$ at the first measurement is not conditioned on any previous measurement. Each separate density in Equation 3.11 can be written as

$$f_{\underline{U}(t_i)/\underline{Y}(t_i)} = [2\pi^{n/2} P(t_i^+)^{\frac{1}{2}}]^{-1} \exp\{\cdot\}$$

$$\{\cdot\} = -\tfrac{1}{2}[\underline{\xi} - \hat{\underline{U}}(t_i^+)]^T P(t_i^+)^{-1} [\underline{\xi} - \hat{\underline{U}}(t_i^+)] \qquad 3.12$$

where $\underline{U}(t_i^+)$ and $P(t_i^+)$ are the mean and covariance which are conditioned on the measurement sequence $\underline{Y}(t_i)$ at time t_i and the unknown parameters Θ, and similarly

$$f_{\underline{Y}(t_j)/\underline{Y}(t_{j-1})} = \frac{1}{(2\pi)^{m/2} F(t_j)^{\frac{1}{2}}} \exp\{\cdot\}$$

$$\{\cdot\} = -\tfrac{1}{2}[\underline{y}_j - H\hat{\underline{U}}(t_j)]^T F(t_j)^{-1} [\underline{y}_j - H\hat{\underline{U}}(t_j)] \qquad 3.13$$

where

$$F(t_j) = HP(t_j^-)H^T + R \qquad 3.14$$

By substituting Equation 3.12 and Equation 3.13 back into Equation 3.10, and solving for Equation 3.9a, the solution of the gradients of the likelihood function with respect to $\underline{\xi}$ is

$$-[\underline{\xi} - \hat{\underline{U}}(t_i^+)]^T P(t_i^+)^{-1} \Big|_{\substack{\underline{\xi} = U^*(\underline{\xi}) \\ \theta = \Theta^*(t_i)}} = \underline{0}^T$$

or

$$\underline{U}^*(t_i) = \hat{\underline{U}}(t_i^+) \Big|_{\theta = \Theta^*(t_i)} \qquad 3.15$$

From looking at Equation 3.15, the maximum likelihood estimate of the state $\underline{U}^*(t_i)$ can be obtained by using the Kalman filter algorithm provided that the values of the parameters Θ are the maximum likelihood estimates of the parameters Θ^*.

The same procedures can be applied to Equation 3.9b, the gradient of the likelihood functions with respect to θ. The solution of Equation 3.9b is in Maybeck, Vol. II, Chapter 10. A closed form solution of Equation 3.9b generally is not possible. An iterative algorithm will have to be used.

Newton-Raphson Algorithm

The Newton-Raphson technique was used to find the best estimates of the parameters Θ^* denoted by $\hat{\theta}^*(t_i)$. The Newton-Raphson equation can be written as

$$\hat{\theta}^*(t_i) = \hat{\theta}_*(t_i) - \nabla_\theta^2 L[\hat{\underline{U}}_*(t_i), \hat{\theta}_*(t_i); \underline{\mathbf{y}}_i]^{-1} \cdot \nabla_\theta L[\hat{\underline{U}}_*(t_i), \hat{\theta}_*(t_i); \underline{\mathbf{y}}_i]^T$$

where $\hat{\theta}_*(t_i)$ is the previous estimate, and $L[\hat{\underline{U}}_*(t_i), \hat{\theta}_*(t_i); \underline{\mathbf{y}}_i]$ is the likelihood function evaluated using $\hat{\underline{U}}_*(t_i)$ (the best estimate of the temperature profile from the Kalman estimator using the best available parameter estimates $\hat{\theta}_*(t_i)$) and $\hat{v}_*(t_i)$.

Unfortunately, Equation 3.16 involves solving a second order partials differential equation, and the computation will be enormous. An approximation called "scoring" was suggested by Rao (Ref. 15) which simplifies the computation substantially. The accuracy of the computation can be maintained as long as the "number of samples is large". (Ref. 2,14,15) The approximation is

$$\nabla_\theta^2 L[\hat{\underline{U}}_*(t_i),\hat{\theta}_*(t_i);\underline{\mathbf{y}}_i] \cong -J[t_i,\hat{\underline{U}}_*(t_i),\hat{\theta}_*(t_i);\underline{\mathbf{y}}_i] \qquad 3.17$$

where $J[\cdot]$ is called the conditional information matrix given by

$$J[t_i,\hat{\underline{U}}_*(t_i),\hat{\theta}_*(t_i);\underline{\mathbf{y}}_i] = E\{\nabla_\theta L\hat{\underline{U}}_*(t_i),\theta;\underline{\mathbf{y}}_i]$$
$$\nabla_\theta L[\hat{\underline{U}}_*(t_i),\theta,\underline{\mathbf{y}}_i]^T\}_{\theta=\hat{\theta}} \qquad 3.18$$

Therefore, with the approximation, the computation of Equation 3.16 will only involve the evaluation of the first order partials, and Equation (3.16) becomes

$$\hat{\theta}^*(t_i) = \hat{\theta}_*(t_i) + J[t_i,\underline{U}_*(t_i),\hat{\theta}_*(t_i);\underline{\mathbf{y}}_i]^{-1}$$
$$\cdot \nabla_\theta L[\hat{\underline{U}}_*(t_i),\hat{\theta}_*(t_i);\underline{\mathbf{y}}_i] \qquad 3.19$$

where the K^{th} term of the first order derivative can be approximated by (Ref. 2)

$$\frac{\partial}{\partial\theta_k} L[\underline{U}_*(t_i),\hat{\theta}_*(t_i);\underline{\mathbf{y}}_i] = \sum_{j=1}^{i} \frac{\partial\hat{\underline{U}}(t_j)^T}{\partial\theta_k} \cdot \{\cdot\}$$

$$\{\cdot\} = H^T[HP(t_j^-)H^T + R]^{-1}\{\underline{\mathbf{y}}_j - H\hat{\underline{U}}(t_j)\} \qquad 3.20$$

where $\frac{\partial \hat{\underline{U}}(t_j^-)^T}{\partial \theta_K}$ is the sensitivity which can be evaluated by taking the partials of Equation 2.3 with respect to the parameter θ_K, (see Appendix B) where K = 1,2,3 ··· P.

The "conditional information matrix" can also be approximated by

$$J_{kl} = \sum_{j=1}^{i} \frac{\partial \hat{\underline{U}}(t_j^-)^T}{\partial \theta_k} H^T F^{-1}(t_j) H \frac{\partial \hat{\underline{U}}(t_j^-)}{\partial \theta_l} \qquad 3.20$$

where J_{kl} is the kl^{th} element of the P x P matrix. The $\frac{\partial \hat{\underline{U}}(t_j^-)}{\partial \theta_k}$ is the "a priori" sensitivity propagated from "a posteriori" sensitivity $\frac{\partial \hat{\underline{U}}(t_{j-1}^+)}{\partial \theta_k}$ or simply

$$\frac{\partial \hat{\underline{U}}(t_j^-)}{\partial \theta_k} = \frac{\partial \hat{\underline{U}}(t_{j-1}^+)}{\partial \theta_k} \qquad 3.21$$

The "a posteriori" sensitivity can be evaluated by

$$\frac{\partial \hat{\underline{U}}(t_j^+)}{\partial \theta_k} = [I - K(t_j)H] \frac{\partial \hat{\underline{U}}(t_j^-)}{\partial \theta_k} \qquad 3.22$$

Therefore, the sensitivity is updated and propagated through the entire sample time history. With the information provided by the "score" vector and the "conditional information matrix", the best estimate of the parameters can be found. Finally, the best estimate of the parameters will then be used in the Kalman state estimator to propagate the temperatures. The iteration will continue until the last iteration is reached, and hopefully, the parameters will already be converged to the optimal values.

A Summary of the Data Reduction Technique

The whole data reduction technique is summarized in Figure 4. The process is characterized by four steps. First, initial conditions usually were generated by first running a small segment of the maneuver and using the output of the process as initial conditions. Constant initial conditions are assumed for the first small segment, and initial sensitivities $\nabla_{\theta}\hat{\underline{U}}(t_o)$ are assumed to be zero. The initial covariance for the second time segment are usually reinstated to the values given in the error models. Second, with these initial conditions, temperatures, covariance, and sensitivities can be estimated using Equation 3.2, Equation 3.3, and the sensitivities equation derived in Appendix B. Since Equation 3.2 only involved solving the deterministic part of the model, a method described in Williams (Ref. 18) can be used. First, the time rate of change of temperature is approximated with a first order backward difference given by

$$\dot{\underline{U}} = [\underline{U}(t_n) - \underline{U}(t_{n-1})]/\Delta t \qquad 3.23$$

Since the radiation term is the only nonlinear term, a special iterative method was used. A Newton-Raphson iteration technique with a quadratic extrapolation scheme which is described fully in Williams was used to solve Equation 2.3a, the surface boundary condition. Therefore, with the surface temperature known, the rest of the temperature profile, n-1, can be solved. This method has been found to be more efficient than solving Equation 3.2 which has also been linearized.

The next step is to update the estimates using Equation 3.5 to Equation 3.7 and Equation 3.22. This procedure is repeated and propagated up to time t_i, the end of a time segment. In addition, the score and the conditional information matrix will be generated by adding up the sensitivity estimates. Last, the parameters can then be updated with the information provided by the score and the conditional information matrix. Finally, the whole process is then started all over again and this time with the new initial conditions.

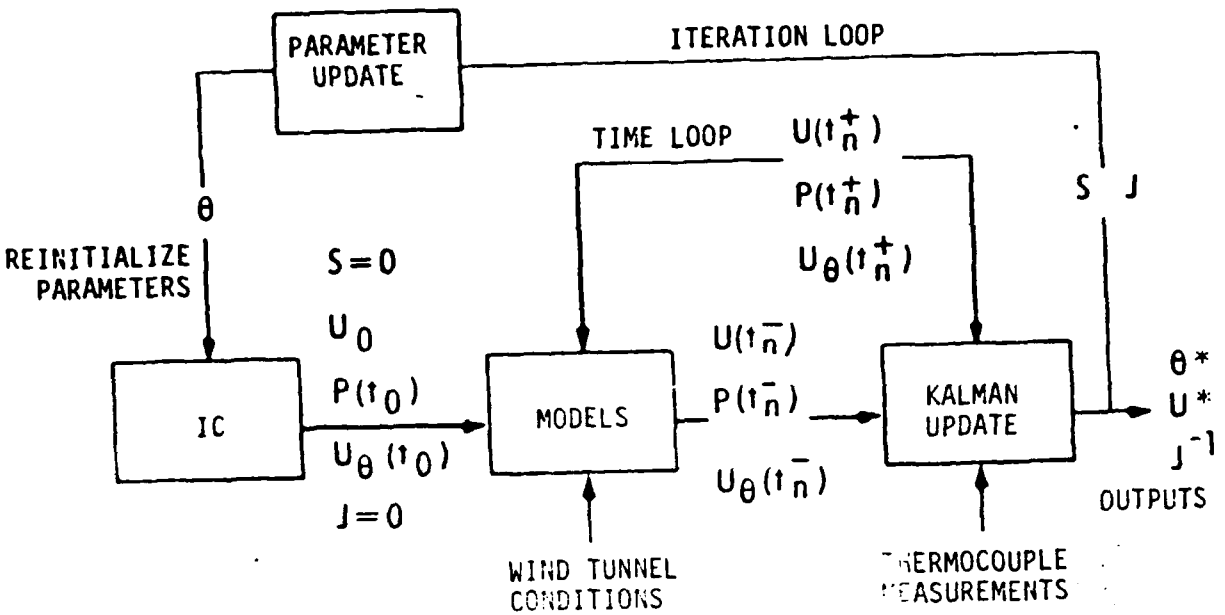

Figure 4 A Summary of the Data Reduction Technique

IV. Wind Tunnel Result

Physical Wind Tunnel Test Articles Descriptions

A wind tunnel test was conducted by the AFWAL in support of AFFTC. The experiment is conducted in a Mach 14 wind tunnel. The purpose is to simulate the flow field of the Space Shuttle Orbiter during reentry.

The primary wind tunnel model consisted of a 15 inche long, 7 inche wide, and 2 inche thick stainless steel plate. One important feature in this model is a 6 inch square cut-out which is used to hold test samples. The test articles consisted of the Space Shuttle HRSI tile and the FRSI material and thin skin stainless steel article. (See Figures 5, 6, 7) Thermocouples are imbedded at numerous locations in the test articles as shown in the figures. The complete flat plate model is then mounted on a support bracket which in turn is mounted on the pitch sector.

A remote shock generator was also used for some test runs. Since shock generated data was not used, a description of this model was not necessary. A water cooled surface which is shown in Figure 8 was used with Space Shuttle articles. This article is mounted above the flat plate model. This surface will provide a known temperature which heat from the flat plate model is radiated to.

Therefore, with the primary flat plate model, thermocouple measurements were obtained by pitching the model with transient and steady state maneuvers.

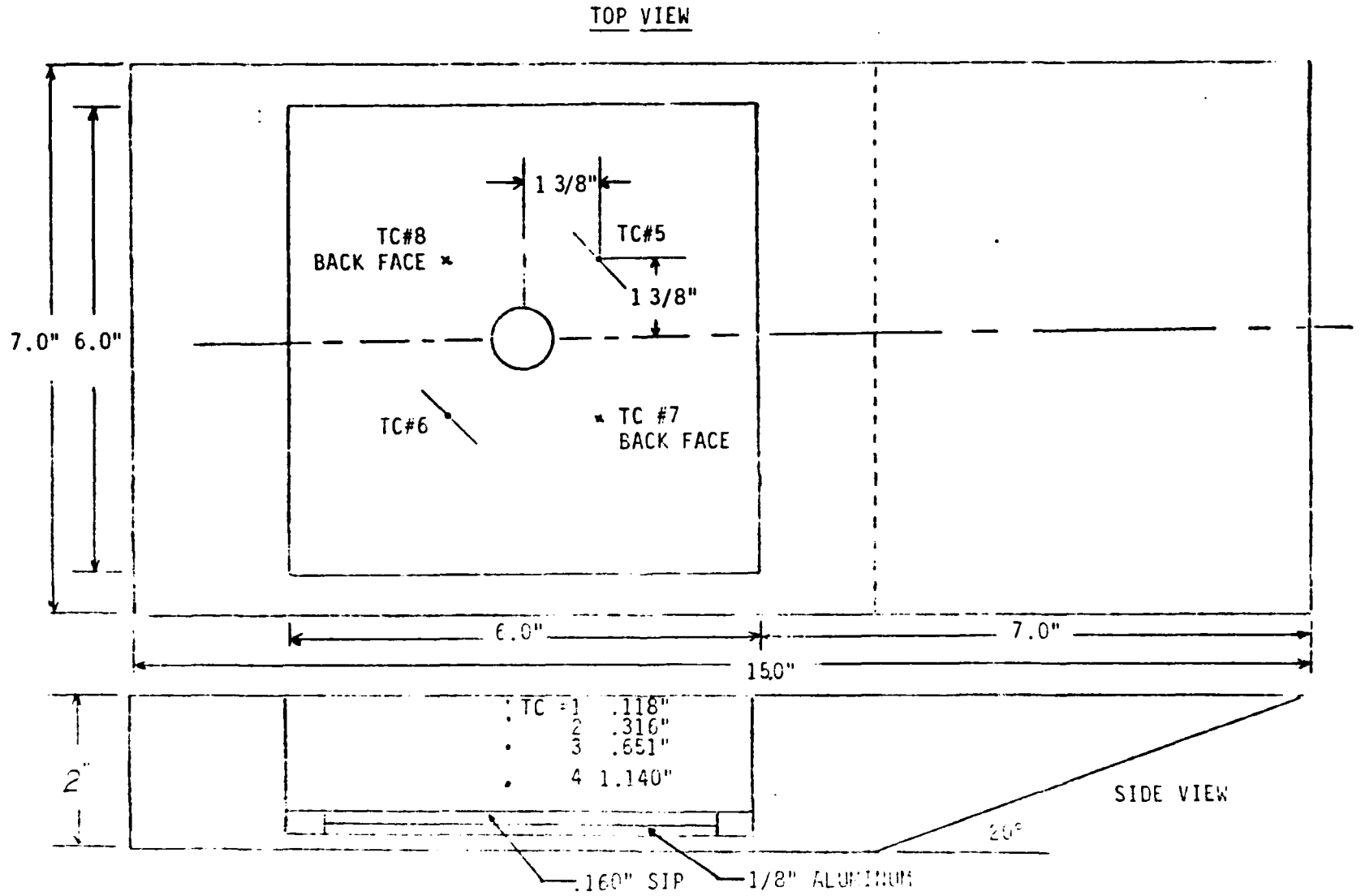

Figure 5 HRSI Test Article Layout

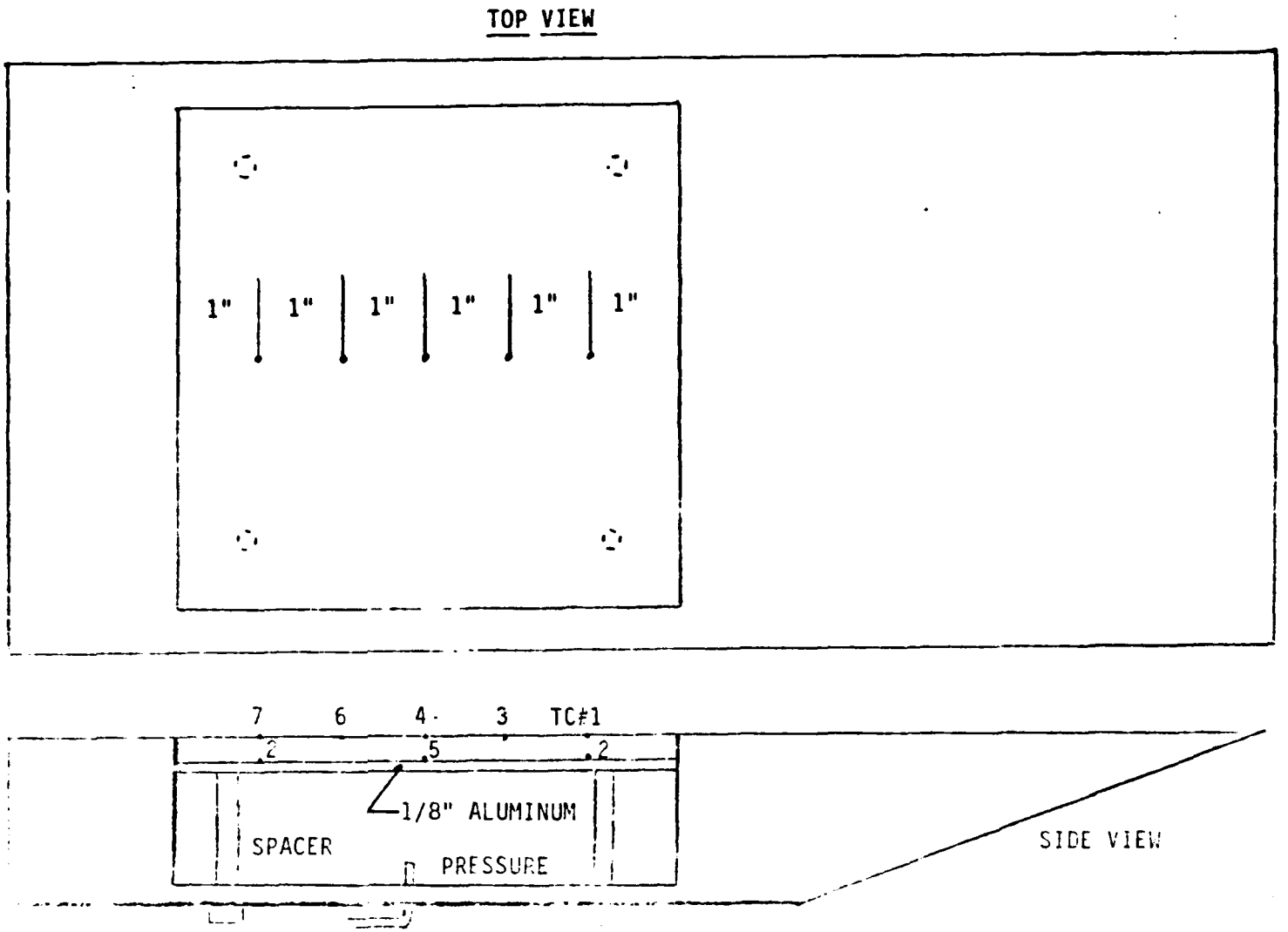

Figure 6 FRSI Test Article Layout

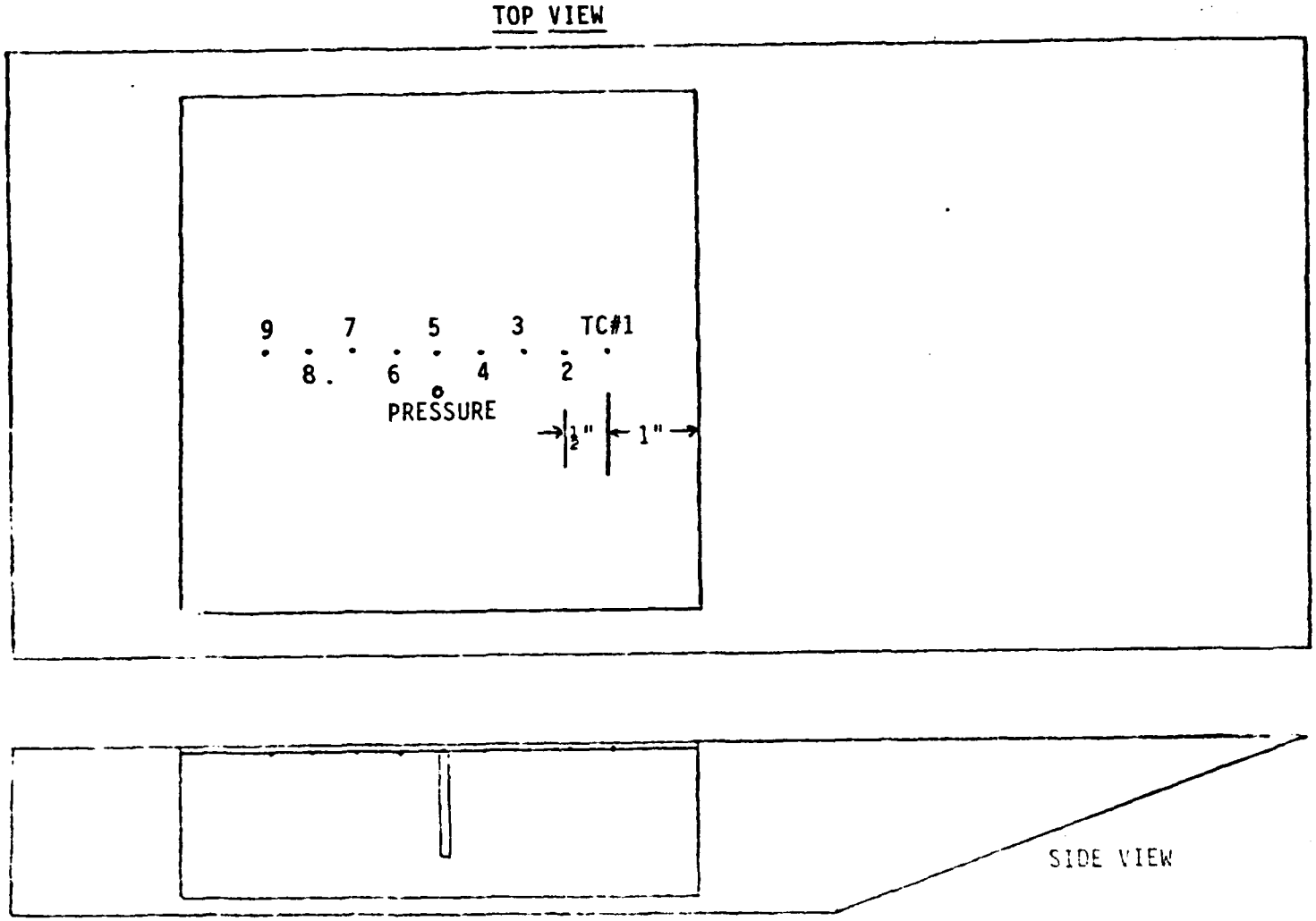

Figure 7 Thin Skin Test Article Layout

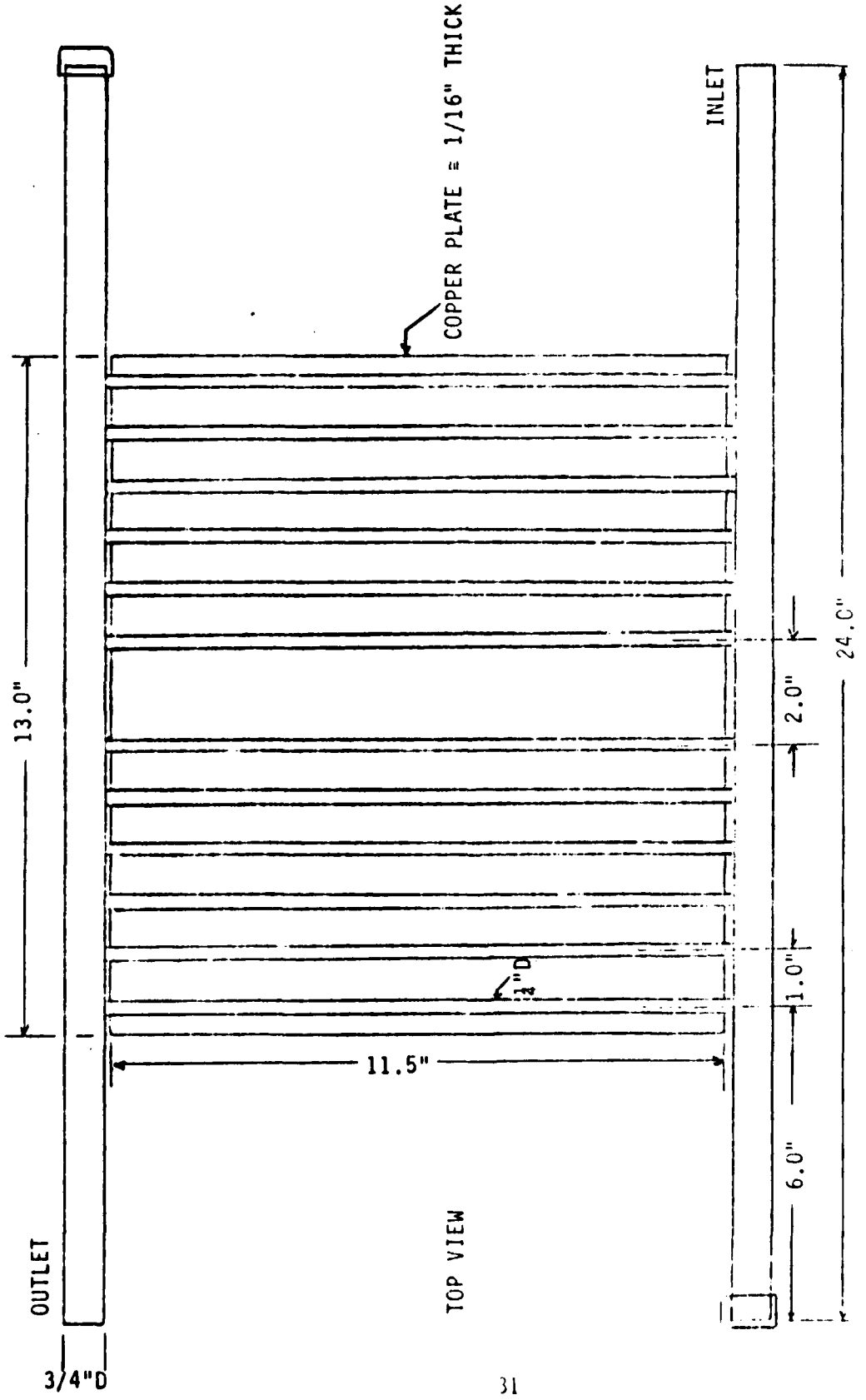
COPPER PLATE = 1/16" THICK
INLET
13.0"
2.0"
24.0"
1.0"
1/4"D
11.5"
6.0"
OUTLET
3/4"D
TOP VIEW

HRSI Wind Tunnel Results and Discussion

A systematic approach was used to reduce the HRSI data. There are three steps in this process. First, a transient maneuver of the HRSI data will be reduced to estimate the heating and thermal parameters. Second, the steady state and transient data will be reduced and compared. Last, a comparison between the HRSI data and the available thin skin data and also with the Eckert theory should demonstrate the feasibility of the transient maneuver technique.

A transient maneuver was analyzed. The maneuver time history and the temperature time history are shown in Figure D-1. The maneuver pitched the model from 14 degrees to 3 degrees continuously. (See Appendix C) The main purpose for analyzing this maneuver was to identify the necessary heating parameters and the thermal parameters. A surface thermocouple was used for implementation to "HEATEST". For some reason, the parameters were trading with one another, and the "HEATEST" wasn't able to estimate the parameters. One reason might be that error is present in the measurements that was not accounted for in the mathematical models.

One way to show if error exists in the measurements is to let the temperature propagate without updating by the Kalman filter. Heating and thermal parameters were fixed similar to a simulator. Several values for the parameters were used to generate the temperature time history. The temperature time history that tracked closely with the thermocouple measurements is shown in Figure D-2. The time history shows a lag in the thermocouple measurements of approximately three seconds. Three seconds lag is unrealistically high to be accounted for

by anything in the present models. This has shown that errors do exist in the system, and the error could be in either the mathematical models or in the measurements obtained from the real system. Further investigation will be necessary.

Small time segments of maneuver one were generated, and the results were correlated manually. The segments are shown in Figure D-3. One assumption that was made is that segments containing steady state deflection angle should correlate well with one another. Furthermore, segments that are away from the wind tunnel start up and away from the transient maneuver should correlate very well. This assumption came from inspection of Figure D-2. The time history tracks very well with the measurement data except at the initial wind tunnel start up and at the transient maneuver. The results of the analysis are shown in Figure D-4 to Figure D-6. Several interesting results were apparent. First, the results indicate that the coating thickness is best approximated to be .001 ft since further decrease of the thickness will not change the correlation very much. The thickness was expected to be between .000833 ft and .00125 ft. However, this test article has been tested numerous times in an arc jet. Although the segments correlate well compared with the other configurations, the transient error still shows up in the figures. Second, the only effect that shows up in the figures by changing the thermal conductivity factor is the magnitude. The worst case based on atmospheric pressure as opposed to the pressure measurement at the base of the tile seems to be with a thermal conductivity factor of three. This also shows up in the steady state correlation which is shown in Figure D-7

and Figure D-8. Therefore, the convective heating parameters were estimated with coating thickness of .001 ft and thermal conductivity factor of one.

The analysis so far indicates that the error is generated in the measurement data. Conversely, this could mean that the real system was not modelled correctly by the present mathematical model.

The next step was to reduce the steady state runs. The time history is shown in Figure D-9 and Figure D-10. One attempt was made to estimate the coating thickness. The estimates were in the range of .00097 ft and .00102 ft. The results further confirm the coating thickness estimate from the previous investigation. An attempt was made also to estimate the thermal conductivity factor, but was not successful. To further confirm the coating thickness estimate, the Kalman filter was turned to see if the optimal estimate was indeed reached. The result of the steady state run with 14 degree deflection angle is tabulated in Table D-I. The results indicate that the coating thickness estimate was an optimal estimate.

Several transient maneuvers were also analyzed using the estimated thermal parameters. The time history of the maneuvers are shown in Figure D-11 to Figure D-13. The procedure used in the first analysis with the heating and thermal parameters fixed similar to a simulator run was also used to analyze the maneuvers. The lag in the temperature time history also shows up in all the maneuvers analysis. (See Figure D-14 to Figure D-15) By looking at these figures, the lag seemed to be reduced with less maneuvers. Even though the lag didn't show up in Figure D-15, the lag is there, but it is small. This should confirm that the lag in the measurements is caused by the transient effect

The results of the transient and steady state were compared with the available thin skin data and also with the Eckert flat plate theory. The comparison is shown in Figure D-16. First of all, the comparison between transient and steady state were relatively good. This indicates that steady state testing technique can be replaced by the transient testing method. But the comparison between HRSI results and thin skin data and Eckert flat plate theory indicates a large discrepancy. There are two possibilities that might have caused the discrepancy. First, a bad measurement device might have caused the lower temperature measurements, and this in turn caused the lower heat rate. Second, the non-isothermal wall effect could have contributed to the lower heat rate. (Ref. 4) Since the leading edge is stainless steel which is a heat sink type material, temperatures on the stainless steel should be less than the temperature on the HRSI tile. Therefore, the lower temperature at the leading edge could affect the temperature on the HRSI which in this case, lowers the heat rate on the HRSI. Nonetheless, these two possibilities needed further investigation.

The heating parameter estimates of maneuver one with the Kalman filter turned on were compared with the estimates with the Kalman filter turned off. Slope and magnitude of the heating estimates with the filter off were higher as shown in Figure D-2. The slope and magnitude estimate with the filter on agree well with steady state results as shown in Figure D-16. Since the heating estimates with the Kalman filter on match the heating estimates with the steady state cases, the estimates with the Kalman filter are believed to be better. To show this, heating parameters of maneuver one were fixed similar to a simulator run using the heating estimates from Figure D-16. The result is shown in Figure D-17. The

result clearly shows that the deviation between the a priori temperature estimates and the temperature measurement is minimized, particularly the slopes of the time histories. Since the slopes of the temperature time histories indicated the correct heating rate, the Kalman filter does optimize the temperature and the heating parameter estimates.

FRSI Wind Tunnel Results and Discussion

Since there is only one thermocouple location available in the HRSI tile, data for the FRSI was used because thermocouples were available in several locations throughout the tile. First of all, a thermocouple at the same location as in HRSI was needed to confirm the validity of the measurement device in the HRSI. One thermocouple available was a little closer to the leading edge of the test article. The thermocouple is denoted as TC 1 in Figure 6. A bondline thermocouple was also used. Since the FRSI has a smaller number of nodes, an additional bondline thermocouple will not increase computational time too much. The result should give a very good indication of how good the thermocouple measurement device was used in the HRSI analysis. Second, thermocouples at two more locations were used. (See Figure 6 for TC4, TC5, TC7 and TC8) If the non-isothermal wall in fact caused the discrepancy, the effect should be less as the distance between measurement and the leading edge is larger. From these two analyses, a better understanding of the discrepancy will be possible.

With the previous experience, steady state runs were analyzed first. The time history for the steady state runs are shown in Figure D-18 and Figure D-19. The heating parameters were estimated at each thermocouple locations. The heating parameters estimates at the first location which is closest to the leading edge came to be about the same

magnitude as in the HRSI results. This has demonstrated that the thermocouple measurement is valid. This also confirmed that the discrepancy previously noted was not caused by instrumentation errors. The magnitude of the heat rate estimates increased as the location became further away from the leading edge. Thus, the results confirm the assumption for non-isothermal wall effect, that as the distance between the non-isothermal wall becomes large, the effect should be less. One other interesting result was that the coating thickness is very sensitive to the error in the models even in the steady state runs. In this case, the error is caused by the non-isothermal wall effect. On the other hand, the coating thickness could be lower at the leading edge since the coating was applied on by hand. Therefore, no conclusion will be drawn from this.

One transient maneuver run was analyzed for completeness. The time history is shown in Figure D-20. The results also were similar to the steady state results. The comparison between FRSI Results and Thin Skin and Eckert theory is shown in Figure D-21. Comparing the HRSI and FRSI results at a similar TC location, the heating rate of the FRSI is higher than the heating rate of the HRSI. The reason is that the specific heat of the FRSI coating is higher than the HRSI coating. Thus, the FRSI surface temperature will respond slower than the HRSI and will cause a smaller temperature step at the interface between the stainless steel. Therefore, the non-isothermal wall effect should be less.

To show the transient error caused by the non-isothermal wall effect as shown in the HRSI analysis. The heating and thermal parameters were fixed similar to the HRSI analysis. The results are shown in Figure D-22. The results have indicated the transient effect is less

as the non-isothermal wall effect is also less. This confirms that the transient error is caused by the non-isothermal wall effect also. The discrepancy is also investigated by Cappelano (Ref. 4), and his results are similar. Furthermore, a similar effect has shown up in the flight thermocouple data analysis. (Ref. 11) The analysis was on the FRSI on the Orbital Maneuvering System (OMS) pods. The FRSI location was approximately six inches downstream of LRSI tiles. A three second time skew was required to correlate the flight data, which is similar to the three second skew in the wind tunnel analysis.

One last investigation on the sample rate effect has confirmed the approximation made using the scoring assumption. Sample rate has been varied from one sample per second to five samples per second. The results of the parameter estimates are shown in Table D-II. The higher the sample rate the better the convergence to the optimal parameter estimates.

V. Conclusion and Recommendation

Conclusion

The feasibility of the transient maneuver testing technique has been demonstrated using the wind tunnel HRSI and FRSI data. The results also demonstrated the feasibility of the data reduction method. The Kalman filter enhanced the heating parameter estimates even though a modelling error was identified. Without the Kalman filter, the heating estimates did not agree well with steady state results. The biggest modelling error was believed to be caused by the non-isothermal wall effect. This can explain some of the questions raised by the flight data analysis. One example would be on the OMS. Furthermore, the transient lag or the three second skew on the HRSI data analysis also was found to be due to non-isothermal wall effect. This can be eliminated if the same material was used throughout in the test models. Nonetheless, the overall results indicated the transient maneuvers testing technique is feasible. Further development of the technique should enhance the flight test capability and also enhance future wind tunnel testing.

Recommendation

Since the non-isothermal wall effect caused most of the modelling error, a new test model with the same material properties should be used for future wind tunnel tests. Different materials with different material properties should be avoided in order to avoid the non-isothermal wall effect. Thermocouples at various locations are necessary to confirm the assumption of the non-isothermal wall effect. For example, without the non-isothermal wall effect, the result should be consistent at various locations. One last thing, even if the transient test technique has

been found to be feasible in wind tunnel or in flight test, several steady state maneuver runs should be included in the wind tunnel test. This might be important because some parameters might be best estimated by steady state maneuvers. For example, coating thickness was best estimated using steady state runs. This is due to the fact that the temperature in the wind tunnel test does not reach equilibrium as fast as the flight test. Finally, because the thermal conductivity depends on the pressure in the test article, the pressure sensors in the test articles should be sealed to minimize the uncertainty in the estimates.

Bibliography

1. Åstrom, K.J., "Maximum Likelihood and Prediction Error Methods," Automatica, Vol. 16, PP551-576, (1980).

2. Audley, David R. and James K. Hodge, "Identifying the Aerothermodynamic Environment of the Space Shuttle Orbiter Columbia," Sixth IFAC Symposium on Identification and System Parameter Estimation (June 1982).

3. Beck, James V., "An Analytical and Experimental Study for Surface Heat Flux Determination," Journal of Spacecraft and Rockets, Vol. 15, No. 6, PP381-382, (November-December, 1978).

4. Cappelano, Peter T. Heat Transfer/Boundary Layer Investigation Heating Model Discrepancies in Wind Tunnel Testing of Orbiter Insulating Articles. MS Thesis. Wright-Patterson AFB, Ohio: Air Force Institute of Technology, December 1982. (AFIT/GA/AA/82D-3)

5. Davenport, Wilbur B., Jr. Probability and Random Processes. New York: McGraw-Hill Book Company, 1970.

6. Dunbar, Bonnie J., "A New Era in Transportation," American Ceramic Society Bulletin, Vol. 60, PP1180-1187, (November 1981).

7. Eckert, E.R.G., "Survey of Boundary Layer Heat Transfer at High Velocities and High Temperatures", WADC TR59-624, (1960).

8. Eykhoff, Pieter. System Identification, New York: John Wiley and Sons, 1974.

9. Gebharf, Benjamin. Heat Transfer (Second Edition), New York: McGraw-Hill Book Company, 1971.

10. Hodge, James K., Paul W. Phillips, and David R. Audley, "Flight Testing a Manned Lifting Reentry Vehicle (Space Shuttle) for Aerothermodynamic Performance," AIAA/SETP/SFTE/SAE/ITEA/ and IEEE, Flight Testing Conference, 1st, AIAA-81-2421, (November 11-13, 1981).

11. Hodge, J.K., D.R. Audley, P.W. Phillips and E.K. Hertzler," Aerodynamic Flight Envelope Expansion for a Manned Lifting Reentry Vehicle (Space Shuttle)", Flight Mechanics Symposium on "Ground/ Flight Test Techniques and Correlation," Paper No. 3A, AGARD, (October 1982).

12. Jazwinski, Andrew H. Stochastic Process and Filtering Theory. New York: Academic Press, 1970.

13. Korb, L.J., C.A. Morant, R.M. Calland, and C.S. Thatcher, "The Shuttle Orbiter Thermal Protection System," American Ceramic Society Bulletin, Vol. 60, PP1188-1193, (November, 1981).

14. Maybeck, Peter S. Stochastic Models, Estimation, and Control. New York: Academic Press Inc., Vol. I, II, 1979.

15. Rao, C.R. Advanced Statistical Methods in Brometric Research. New York: John Wiley and Sons, Chapter 4, 1952.

16. Schulz, G. "Maximum Likelihood Identification Using Kalman Filtering-Least Squares Estimation," IFVLR, (August 12, 1975).

17. Throckmorton, "Benchmark Aerodynamic Heat-Transfer Data from the First Flight of the Space Shuttle Orbiter," AIAA paper 82-0003, (January 1982).

18. Williams, S.D. and Donald M. Curry, "An Implicit-Iterative Solution of the Heat Conduction Equation with a Radiation Boundary Condition," International Journal for Numerical Methods in Engineering, Vol. 11, No. 10, PP1605-1619, (1977).

Appendix A

The n-differential equations can be written

$$\dot{\underline{U}}(t) = A\underline{U}(t) + \underline{B} + \underline{W}(t) \qquad A.1$$

where A is the n x n tridiagonal matrix with elements,

$$a_{11} = 2(-K_A/\Delta X_A + 4\sigma\varepsilon U_1^3(t_{n-1}))/C_A\rho_A\Delta X_A$$

$$a_{22} = 2K_A/C_A\rho_A\Delta X_A^2$$

$$a_{21} = 2K_A/\Delta X_A(C_A\rho_A\Delta X_A + C_B\rho_B\Delta X_2)$$

$$a_{22} = -2(K_A/\Delta K_A + K_B/\Delta X_2)/(C_A\rho_A\Delta X_A + C_B\rho_B\Delta X_2)$$

$$a_{23} = 2K_A/\Delta X_2(C_A\rho_A\Delta X_A + C_B\rho_B\Delta X_2)$$

$$a_{i\ i-1} = 2K_B/\Delta X_{i-1}C_B\rho_B(\Delta X_{i-1} + \Delta X_i)$$

$$a_{ii} = -2(K_B/\Delta X_{i-1} + K_B/\Delta X_i)/C_B\rho_B(\Delta X_{i-1} + \Delta X_i)$$

$$a_{i\ i+1} = 2K_B/\Delta X_i C_B\rho_B(\Delta X_{i-1} + \Delta X_i)$$

$$a_{L-2\ L-3} = 2K_B/\Delta X_{L-3}(C_B\rho_B\Delta X_{L-3} + C_C\rho_C\Delta X_C)$$

$$a_{L-2\ L-2} = -2(K_B/\Delta X_{L-3} + K_C/\Delta X_C)/(C_B\rho_B\Delta X_{L-3} + C_C\rho_C\Delta X_C)$$

$$a_{L-2\ L-1} = -2K_C/\Delta X_C(C_B\rho_B\Delta X_{L-3} + C_C\rho_C\Delta X_C)$$

$$a_{L-1\ L-2} = 2K_C/\Delta X_C(C_C\rho_C\Delta X_C + C_D\rho_D\Delta X_D)$$

$$a_{L-1\ L-1} = -2(K_C/\Delta X_C + K_D/\Delta X_D)/(C_C\rho_C\Delta X_C + C_D\rho_D\Delta X_D)$$

$$a_{L-1\ L} = 2K_D/\Delta X_D(C_C\rho_C\Delta X_C + C_D\rho_D\Delta X_D)$$

$$a_{L\ L-1} = 2K_D/C_D\rho_D\Delta X_D^2$$

$$a_{L\ L} = -2K_D/C_D\rho_D\Delta X_D^2$$

$$b_1 = 2(\sigma\varepsilon(3U_1^4(t_{n-1}) + U_\infty^4) + f(\alpha)h_{ref})/C_A\rho_A\Delta X_A$$

$$b_{i+1} = 0$$

Appendix B

$$\begin{Bmatrix} \theta_1 \\ \theta_2 \\ \theta_3 \\ \theta_4 \end{Bmatrix} = \begin{Bmatrix} \Delta X_A \\ \bar{h}_o \\ \bar{h}_\alpha \\ \phi_K K_B \end{Bmatrix}$$

$$\dot{U}_1 = -M_1 U_1 + M_2 U_2 - D_1 - D_2 \qquad B.1$$

$$\dot{U}_2 = M_3 U_1 - M_4 U_2 + M_5 U_3 \qquad B.2$$

$$\dot{U}_i = M_6 U_{i-1} - M_7 U_i + M_8 U_{i+1} \qquad B.3$$

$$\dot{U}_{L-2} = M_9 U_{L-3} - M_{10} U_{L-2} + M_{11} U_{L-1} \qquad B.4$$

$$\dot{U}_{L-1} = M_{12} U_{L-2} - M_{13} U_{L-1} + M_{14} U_L \qquad B.5$$

$$\dot{U}_L = M_{15} U_{L-1} - M_{16} U_L \qquad B.6$$

This is not the only set of unknown parameters in the heat and thermal model, but the only unknown parameters that have been investigated in this report.

$$M_1 = \frac{2K_A}{C_A \rho_A \Delta X_A^2}$$

$$M_2 = \frac{2K_A}{C_A \rho_A \Delta X_A^2}$$

$$M_3 = \frac{2K_A}{\Delta X_A (C_A \rho_A \Delta X_A + C_B \rho_B \Delta X_2)}$$

$$M_4 = \frac{2(\Delta X_2 K_A + \phi_K K_B \Delta X_A)}{\Delta X_A \Delta X_2 (C_A \rho_A \Delta X_A + C_B \rho_B \Delta X_2)}$$

$$M_5 = \frac{2\phi_K K_B}{\Delta X_2 (C_A \rho_A \Delta X_A + C_B \rho_B \Delta X_2)}$$

$$M_6 = \frac{2\phi_K K_B}{\Delta X_{i-1} K_B \rho_B (\Delta X_{i-1} + \Delta X_i)}$$

$$M_7 = \frac{2(\Delta X_i \phi_K K_B + \Delta X_{i-1} \phi_K K_B)}{\Delta X_{i-1} \Delta X_i (\Delta X_{i-1} + \Delta X_i) C_B \rho_B}$$

$$M_8 = \frac{2\phi_K K_B}{\Delta X_i \; C_B \rho_B (\Delta X_{i-1} + \Delta X_i)}$$

$$M_9 = \frac{2\phi_K K_B}{\Delta X_{L-3} (C_B \rho_B \Delta X_{L-3} + C_C \rho_C \Delta X_C)}$$

$$M_{10} = \frac{2(\Delta X_C \phi_K K_B + \Delta X_{L-3} K_C)}{\Delta X_{L-3} \Delta X_C (C_B \rho_B \Delta X_{L-3} + C_C \rho_C \Delta X_C)}$$

$$M_{11} = \frac{2K_C}{\Delta X_C (C_B \rho_B \Delta X_{L-3} + C_C \rho_C \Delta X_C)}$$

$$M_{12} = \frac{2K_C}{\Delta X_C (C_C \rho_C \Delta X_C + C_D \rho_D \Delta X_D)}$$

$$M_{13} = \frac{2(\Delta X_C K_C + \Delta X_C K_D)}{\Delta X_C \Delta X_D (C_C \rho_C \Delta X_C + C_D \rho_D \Delta X_D)}$$

$$M_{14} = \frac{2K_D}{\Delta X_D (C_C \rho_C \Delta X_C + C_D \rho_D \Delta X_D)}$$

$$M_{15} = \frac{2K_D}{\Delta X_D (C_D \rho_D \Delta X_D)}$$

$$M_{16} = \frac{2K_D}{\Delta X_D (C_D \rho_D \Delta X_D)}$$

$$D_1 = \frac{2\sigma\varepsilon (U_1^4 - U_\infty^4)}{C_A \rho_A \Delta X_A}$$

$$D_2 = \frac{2[\bar{h}_0 + \bar{h}_\alpha(\alpha - \alpha_0)]h_{ref}}{C_A\rho_A\Delta X_A}$$

Let $\frac{\partial \dot{U}_i}{\partial \theta_K} = \frac{d}{dt}\frac{\partial U_i}{\partial \theta_K}$ denoted as $\dot{S}_{\theta_{K_i}}$.

Therefore, the ΔX_A sensitivity equations are

$$\dot{S}_{\Delta X_{A_1}} = \frac{-(C_A\rho_A\Delta X_A M_1 - 8\sigma\varepsilon U_1^3)}{C_A\rho_A\Delta X_A} S_{X_1} + \frac{4K_A(U_1 - U_2)}{C_A\rho_A\Delta X_A^3} + \frac{2\sigma\varepsilon(U_1^4 - U_\infty^4)}{C_A\rho_A\Delta X_A^2} + \frac{2f(\alpha)_{ref}}{C_A\rho_A\Delta X_A^2} \quad \text{B.7}$$

$$\dot{S}_{\Delta X_{A_2}} = M_3 S_{\Delta X_{A_1}} - M_4 S_{\Delta X_{A_2}} + M_5 S_{\Delta X_{A_3}} - \frac{2K_A U_1(2C_A\rho_A\Delta X_A + C_B\rho_B\Delta X_2)}{(C_A\rho_A\Delta X_A^2 + C_B\rho_B\Delta X_2\Delta X_A)^2} + \frac{2\Delta X_2 K_A U_2(2C_A\rho_A\Delta X_2\Delta X_A + C_B\rho_B\Delta X_2^2)}{(C_A\rho_A\Delta X_2\Delta X_A^2 + C_B\rho_B\Delta X_2^2\Delta X_A)^2} + \frac{2\phi_K K_B C_A\rho_A\Delta X_2(U_2 - U_3)}{(C_A\rho_A\Delta X_2\Delta X_A + C_B\rho_B\Delta X_2^2)^2} \quad \text{B.8}$$

$$S_{\Delta X_{A_i}} = M_6 S_{\Delta X_{A_{i-1}}} - M_7 S_{\Delta X_{A_i}} + M_8 S_{\Delta X_{A_{i+1}}} \quad \text{B.9}$$

$$S_{\Delta X_{A_{L-2}}} = M_9 S_{\Delta X_{A_{L-3}}} - M_{10} S_{\Delta X_{A_{L-2}}} + M_{11} S_{\Delta X_{A_{L-1}}} \quad \text{B.10}$$

$$\dot{S}_{\Delta X_{A_{L-1}}} = M_{12} S_{\Delta X_{A_{L-2}}} - M_{13} S_{\Delta X_{A_{L-1}}} + M_{14} S_{\Delta X_{A_L}} \quad \text{B.11}$$

$$\dot{S}_{\Delta X_L} = M_{15} S_{\Delta X_{A_{L-1}}} - M_{16} S_{\Delta X_{A_L}} \quad \text{B.12}$$

The $\bar{h}_o$ sensitivity equations are

$$\dot{S}_{\bar{h}_{o_1}} = \frac{-(C_A\rho_A\Delta X_A M_1 + 8\sigma\varepsilon U_1^3)}{C_A\rho_A\Delta X_A} S_{\bar{h}_{o_1}} + M_2 S_{\bar{h}_{o_2}} \frac{-2h_{ref}}{C_A\rho_A\Delta X_A} \quad \text{B.13}$$

$$\dot{S}_{\bar{h}_{o_2}} = M_3 S_{\bar{h}_{o_1}} - M_4 S_{\bar{h}_{o_2}} + M_5 S_{\bar{h}_{o_3}} \quad \text{B.14}$$

$$\dot{S}_{\bar{h}_o} = M_6 S_{\bar{h}_{o_{i-1}}} - M_7 S_{\bar{h}_{o_i}} + M_8 S_{\bar{h}_{o_{i+1}}} \quad \text{B.15}$$

$$\dot{S}_{\bar{h}_{o_{L-2}}} = M_9 S_{\bar{h}_{o_{L-3}}} - M_{10} S_{\bar{h}_{o_{L-2}}} + M_{11} S_{\bar{h}_{o_{L-1}}} \quad \text{B.16}$$

$$\dot{S}_{\bar{h}_{o_{L-1}}} = M_{12} S_{\bar{h}_{o_{L-2}}} - M_{13} S_{\bar{h}_{o_{L-1}}} + M_{14} S_{\bar{h}_{o_L}} \quad \text{B.17}$$

$$\dot{S}_{\bar{h}_{o_L}} = M_{15} S_{\bar{h}_{o_{L-1}}} - M_{16} S_{\bar{h}_{o_L}} \quad \text{B.18}$$

The $\bar{h}_\alpha$ sensitivity equations are

$$\dot{S}_{\bar{h}_{\alpha_{11}}} = \frac{-(C_A\rho_A\Delta X_A M_1 + 8\sigma\varepsilon U_1^3)}{C_A\rho_A\Delta X_A} S_{h_{\alpha_1}} + M_2 S_{h_{\alpha_2}} - \frac{2h_{ref}(\alpha-\alpha_0)}{C_A\rho_A\Delta X_A} \quad \text{B.19}$$

$$\dot{S}_{\bar{h}_{\alpha_2}} = M_3 S_{\bar{h}_{\alpha_1}} - M_4 S_{\bar{h}_{\alpha_2}} + M_5 S_{\bar{h}_{\alpha_3}} \quad \text{B.20}$$

$$\dot{S}_{\bar{h}_{\alpha_i}} = M_6 S_{\bar{h}_{\alpha_{i-1}}} - M_6 S_{\bar{h}_{\alpha_i}} + M_8 S_{\bar{h}_{\alpha_{i+1}}} \quad \text{B.21}$$

$$\dot{S}_{\bar{h}_{\alpha_{L-2}}} = M_9 S_{\bar{h}_{\alpha_{L-3}}} - M_{10} S_{\bar{h}_{\alpha_{L-2}}} + M_{11} S_{\bar{h}_{\alpha_{L-1}}} \quad \text{B.22}$$

$$\dot{S}_{\bar{h}_{\alpha_{L-1}}} = M_{12} S_{\bar{h}_{\alpha_{L-2}}} - M_{13} S_{\bar{h}_{\alpha_{L-1}}} + M_{14} S_{\bar{h}_{\alpha_L}} \quad \text{B.23}$$

$$\dot{S}_{\bar{h}_{\alpha_L}} = M_{15} S_{\bar{h}_{\alpha_{L-1}}} - M_{16} S_{\bar{h}_{\alpha_L}} \quad \text{B.24}$$

The $\phi_K K_B$ sensitivity equations are

$$\dot{S}_{\phi_K K_{B_1}} = \frac{-(C_A \rho_A \Delta X_A M_1 + 8\alpha U_1^3)}{C_A \rho_A \Delta X_A} S_{\phi_K K_{B_1}} \qquad B.25$$

$$\dot{S}_{\phi_K K_{B_2}} = M_4 S_{\phi_K K_{B_1}} - M_4 S_{\phi_K K_{B_2}} + M_5 S_{\phi_K K_{B_3}} + \frac{2(U_3 - U_3)}{\Delta X_2 (C_A \rho_A \Delta X_A + C_B \rho_B \Delta X_2)} \qquad B.26$$

$$\dot{S}_{\phi_K K_{B_i}} = M_6 S_{\phi_K K_{B_{i-1}}} - M_7 S_{\phi_K K_{B_i}} + M_8 S_{\phi_K K_{B_{i+1}}} + \frac{2(\Delta X_i U_{i-1} - (\Delta X_i + \Delta X_{i-1}) U_i + \Delta X_{i-1} U_{i+1})}{\Delta X_i \Delta X_{i-1} C_B \rho_B (\Delta X_{i-1} + \Delta X_i)} \qquad B.27$$

$$\dot{S}_{\phi_K K_{B_{L-2}}} = M_9 S_{\phi_K K_{B_{L-3}}} - M_{10} S_{\phi_K K_{B_{L-2}}} + M_{11} S_{\phi_K K_{B_{L-1}}} + \frac{2U_{L-3}}{\Delta X_{L-3} (C_B \rho_B \Delta X_{L-3} + C_C \rho_C \Delta X_2)} - \frac{2U_{L-3}}{\Delta X_{L-3} (C_B \rho_B \Delta X_{L-3} - C_C \rho_C \Delta X_C)} \qquad B.28$$

$$\dot{S}_{\phi_K K_{B_{L-1}}} = M_{12} S_{\phi_K K_{B_{L-2}}} - M_{13} S_{\phi_K K_{B_{L-1}}} + M_{14} S_{\phi_K K_{B_L}} \qquad B.29$$

$$\dot{S}_{\phi_K K_{B_L}} = M_{15} S_{\phi_K K_{B_{L-1}}} - M_{16} S_{\phi_K K_{B_L}} \qquad B.30$$

The θ_K sensitivity equations can be rearranged in a more convenient linear state space form.

$$\dot{\underline{S}} = C \underline{S} + D \qquad B.31$$

where C is a n x n tridiagonal matrix, and D is a n-dimensional vector.

With this form, a solution of the sensitivity can be found readily. For computer implementation purposes, finite differences were used to approximate the sensitivity. The approximation is

$$\dot{S} = \frac{S^{n} - S^{n-1}}{\Delta t} \qquad \text{B.32}$$

where $\underline{S}^{n-1}$ is the sensitivity at previous time t-1.

Appendix C

HRSI TEST ARTICLE

Maneuver	Run Description
1	α=14°, 10 sec hold, α=3°, no hold, α=14°, hold
2	α=14°, hold, hold, hold
3	α=10°, α=3°, 46 sec hold, α=10°
4	α=10°, α=3°, 12 sec hold, α=14°, 5 sec hold, α=3°, 5 sec hold, α=14°
5	α=14°, 10 sec hold, α=3°, 10 sec hold, α=14°, hold
6	α=14°, 9 sec hold, α=9°, 11 sec hold, α=14°, hold

FRSI TEST ARTICLE

Maneuver	Run Description
7	α=14°, hold, hold, hold
8	α=10°, α=3°, 34 sec hold, α=10°
9	α=14°, α=3°, no hold, α=14°, hold

Appendix D

Table D-I Kalman Filter Tunnings Tabulated Results

SDIC Deviation in Initial Conditions

SDME Deviation in Model

SDMEA Deviation in Thermocouple Measurements

SDBN Deviation of Model Error at Boundary

Maneuver Two

SDIC = .01 SDME = .01 SDMEA = .01

SDBN	ΔX_A	Uncertainty Bound of ΔX_A Estimate	Overall Average Error
.001	.00101	.000076	.048117
.01	.00097	.000082	.0030765
.02	.00097	.0001	.003127
.03	.00097	.00012	.0025332
.04	.00097	.00014	.0019148

SDIC = .01 SDME = .01 SDBN = .01

SDMEA	ΔX_A	Uncertainty Bound of ΔX_A Estimate	Overall Average Error
.001	.00098	.000075	.0012174
.01	.00097	.000082	.0030705
.02	.00096	.000091	.024558
.03	.00096	.0001	.020446

Table D-I Kalman Filter Tunnings Tabulated Results

SDIC = .01 SDMEA = .01 SDBN = .01

SDME	ΔX_A	Uncertainty Bound of ΔX_A Estimate	Overall Average Error
.001	.00096	.000038	.0092017
.01	.00097	.000082	.0030765
.02	.00097	.00014	.0018435
.03	.00097	.0002	.0007917

SDME = .01 SDMEA = .01 SDBN = .01

SDIC	ΔX_A	Uncertainty Bound of ΔX_A Estimate	Overall Average Error
.01	.00097	.000082	.0030765
.02	.00097	.000082	.0044898
.03	.00097	.000082	.0061058

Table D-2 Parameter Estimates for Various Sample Rates

Sample Rate (·/sec)	Iteration 1	2	3	4	5
1	.00083	.00093	.00094	.00095	.00095
2	.00084	.00094	.00095	.00095	.00095
3	.00084	.00094	.00095	.00095	.00095

ΔX_A Estimates (ft)

Sample Rate (·/sec)	Iteration 1	2	3	4	5
1	3.83754	3.99398	4.03160	4.04008	4.04201
2	3.86109	4.01376	4.03896	4.04181	4.04213
5	3.86116	4.0155	4.03204	4.03249	4.0325

$\bar{h}_0$ Estimates (h/h_{ref} at $\alpha_{ref}=14°$)

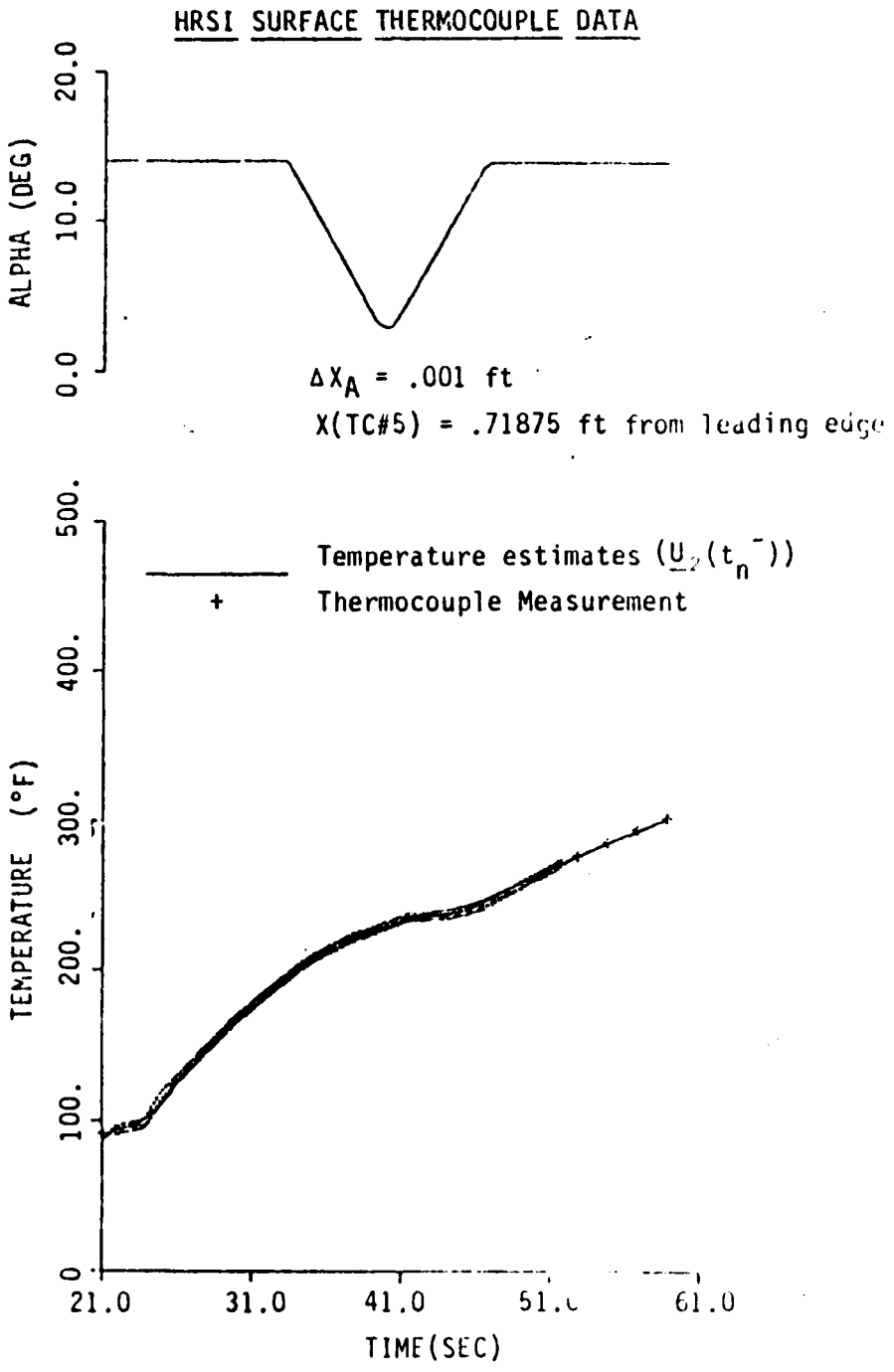

Figure D-1. Deflection Angle and Temperature Time History of Maneuver One

HRSI SURFACE THERMOCOUPLE DATA

X(TC#5) = .71875 ft from leading edge

ΔX_A = .001 ft

$h_o/h_{ref}(\alpha_o = 14^\circ)$ = 2.56

$h\alpha/h_{ref}(\alpha_o = 14^\circ)$ = .150

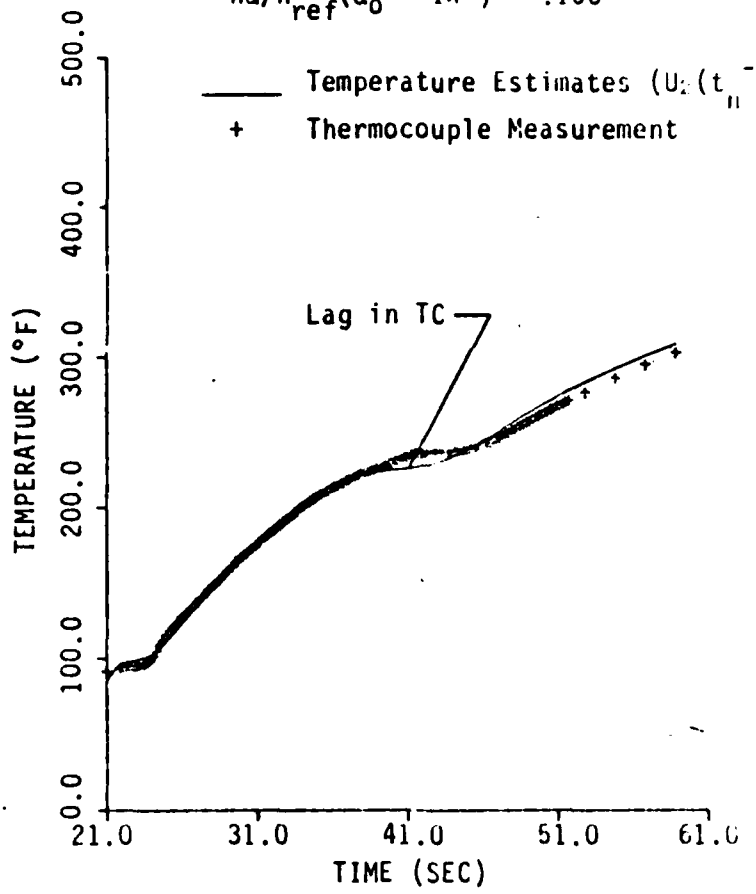

Figure D-2 Temperature Time History of Maneuver One with Parameters Fixed Similar to a Simulator Run

HRSI SURFACE THERMOCOUPLE DATA

SEGMENT	MANEUVERS (α)	SEGMENT	MANEUVERS (α)
1	14°	5	3° to 8°
2	14°	6	8° to 14°
3	14° to 7°	7	14°
4	7° to 3°	8	14°

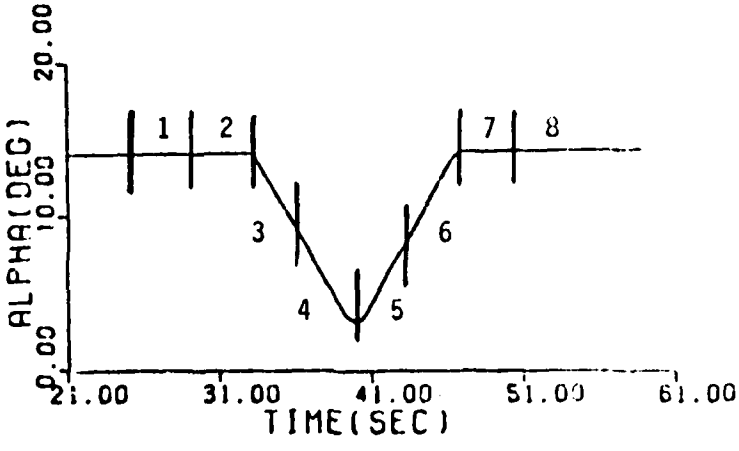

Figure D-3 Small Time Segments History Descriptions of Maneuver One

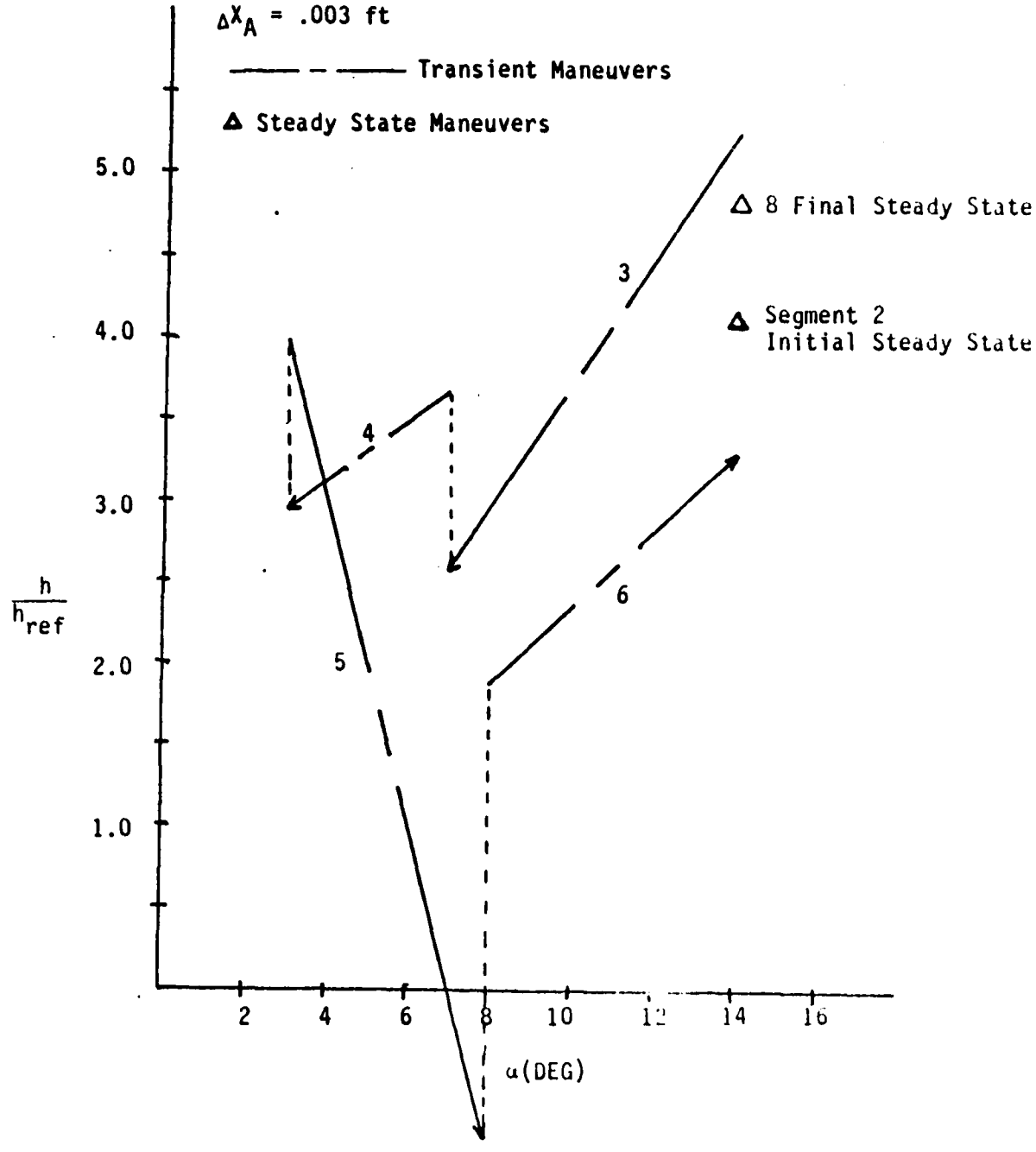

Figure D-4 The Correlation Between Small Time Segments with Coating Thickness of .003 ft

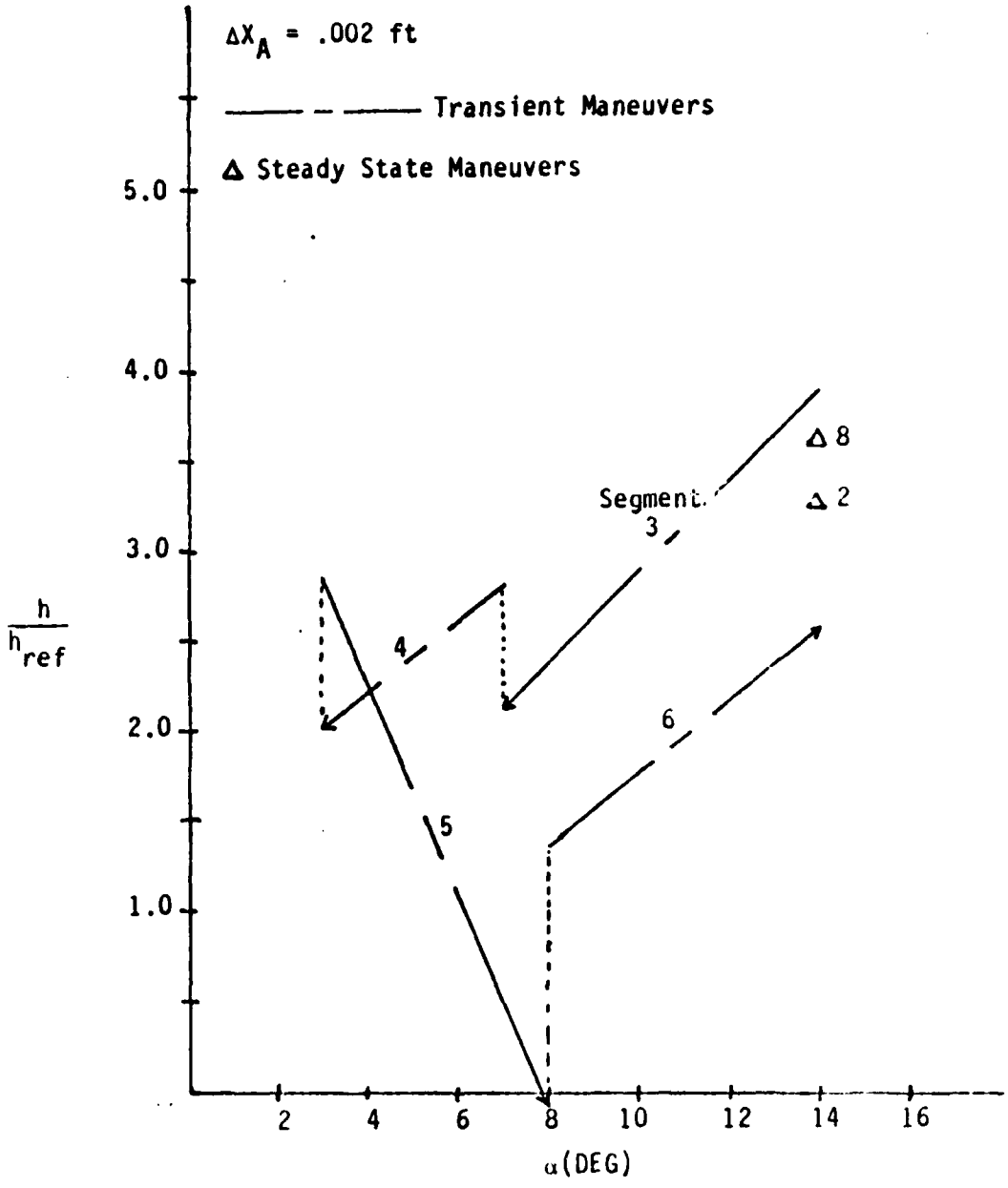

Figure D-5 The Correlation Between Small Time Segments with Coating Thickness of .002 ft

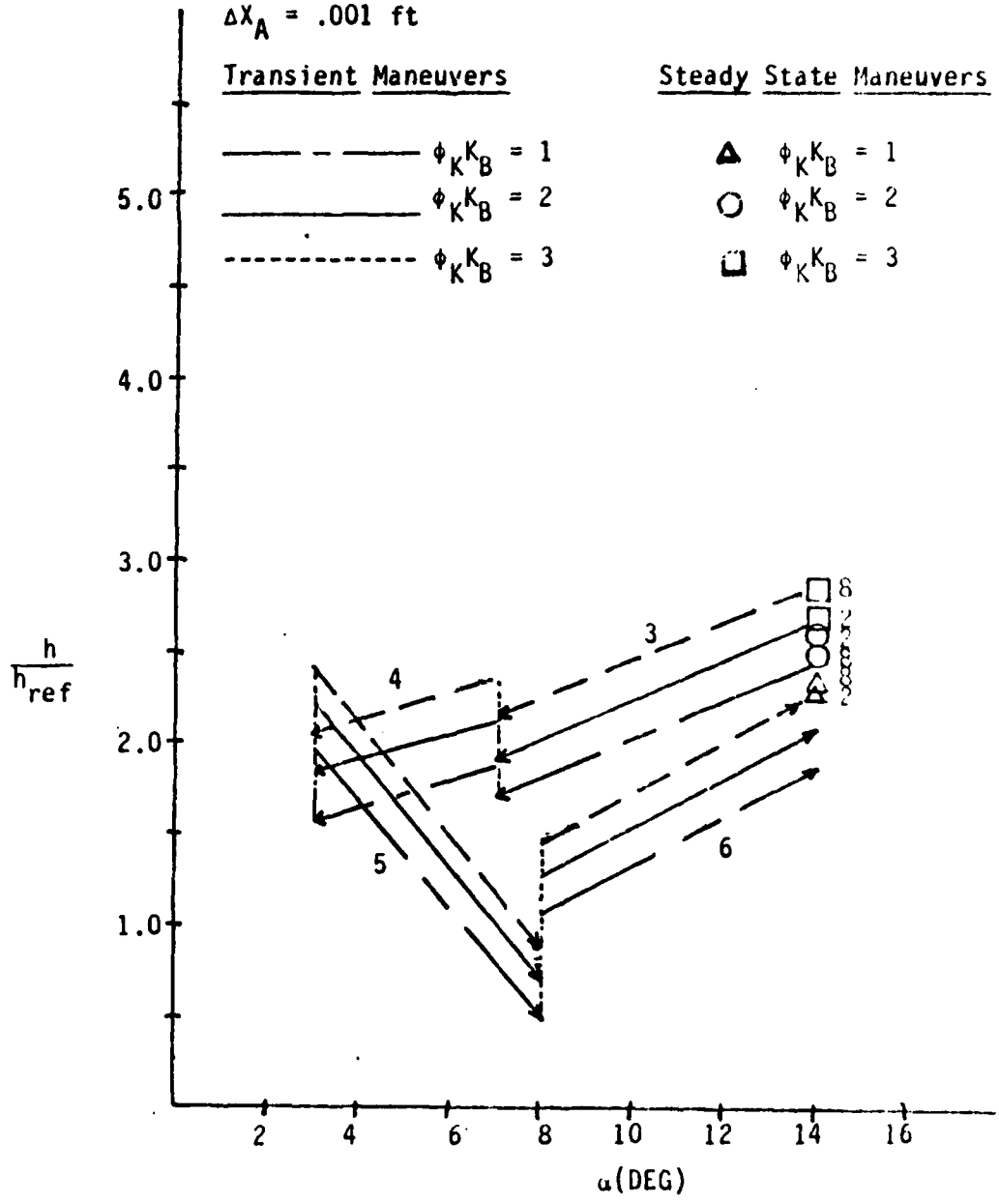

Figure D-6 The Correlation Between Small Time Segments with Coating Thickness of .001 ft

Different Between Segments Two and Eight

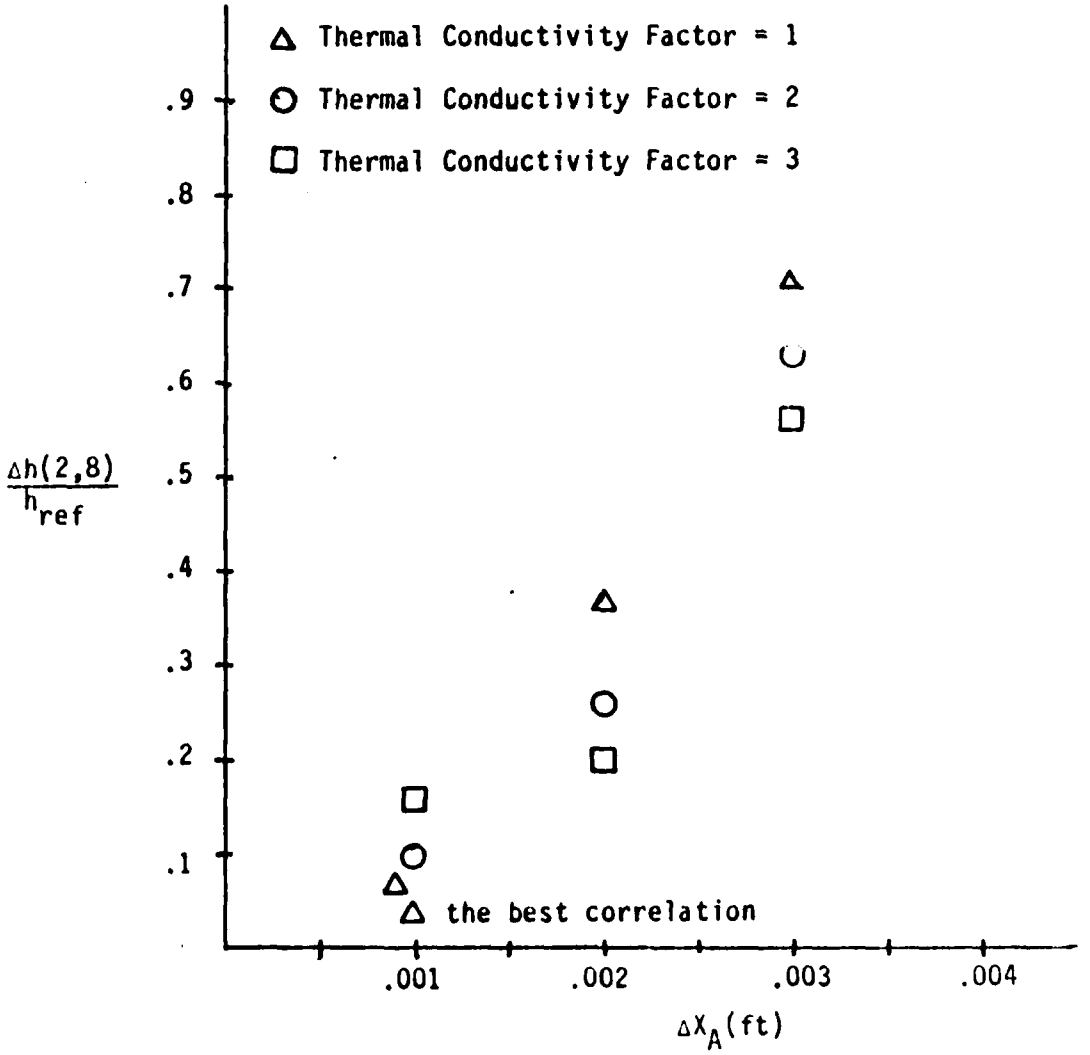

Figure D-7 The Correlation Between Two Steady State Time Segments with Thermal Conductivity Factor Constant

Different Between Segments Two and Eight

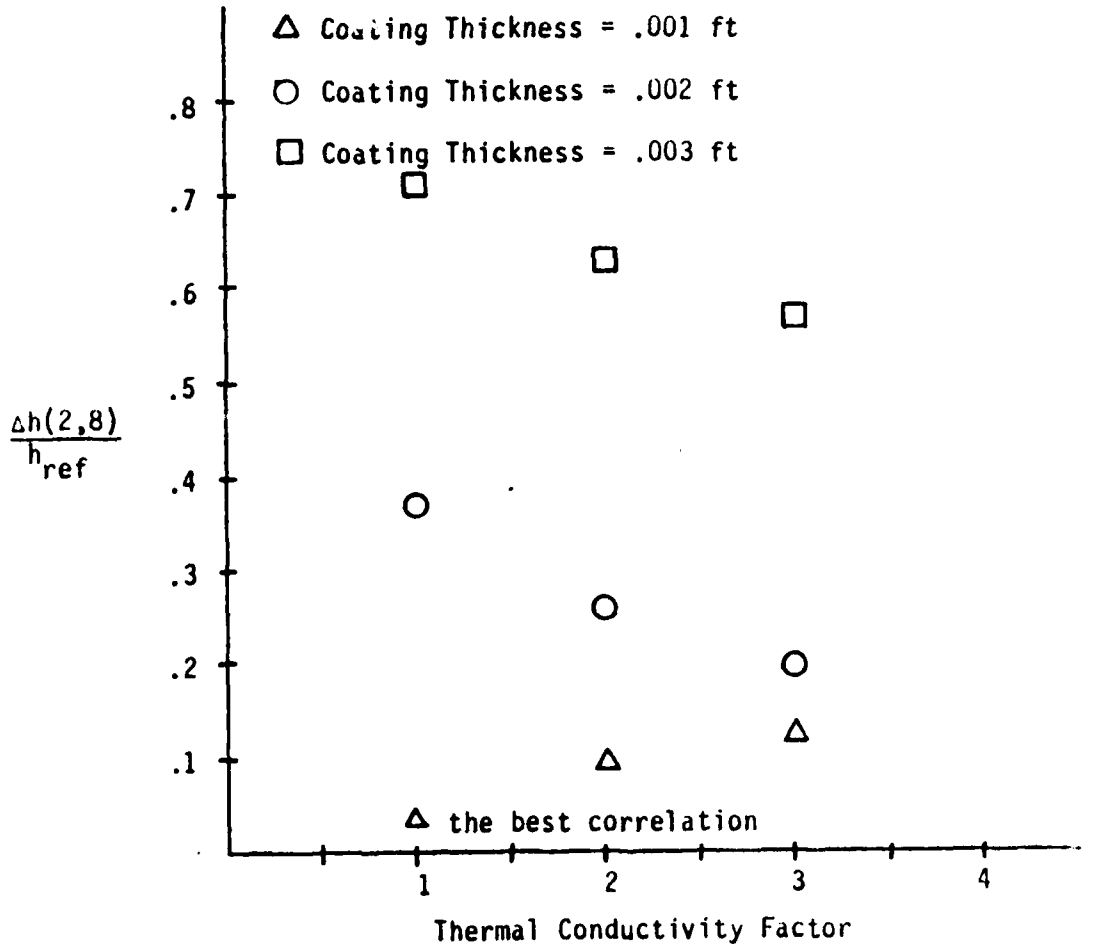

Figure D-8 The Correlation Between Two Steady State Time Segments with Coating Thickness Constant

HRSI SURFACE THERMOCOUPLE DATA

Constant Angle of Attack Equal to 14 Degrees

X(TC#5) = .71875 ft from leading edge

ΔX_A = .001 ft

— Temperature Estimation ($U_2(t_n^-)$)

\+ Thermocouple Measurement

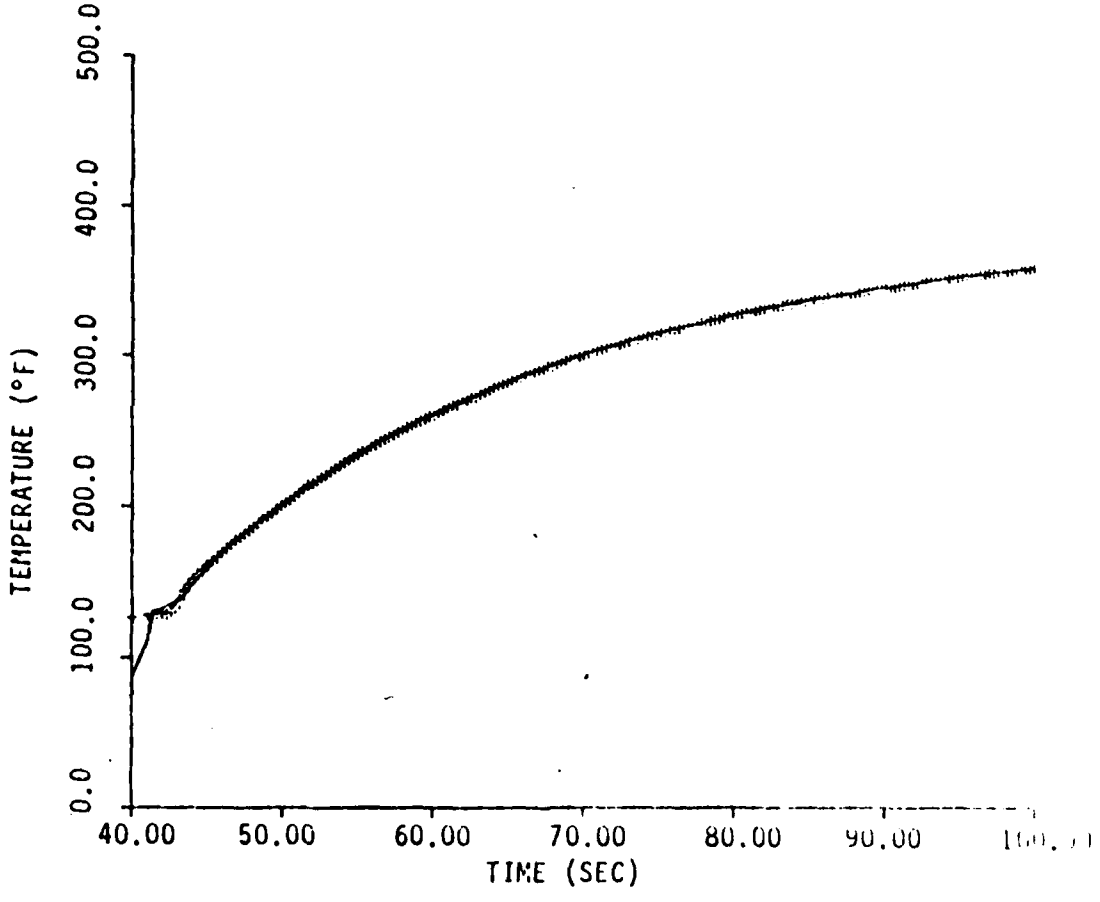

Figure D-9 Temperature Time History of Maneuver Two

HRSI SURFACE THERMOCOUPLE DATA

Constant Angle of Attack Equal to Three Degrees
X(TC#5) = .71875 ft from leading edge
ΔX_A = .001 ft

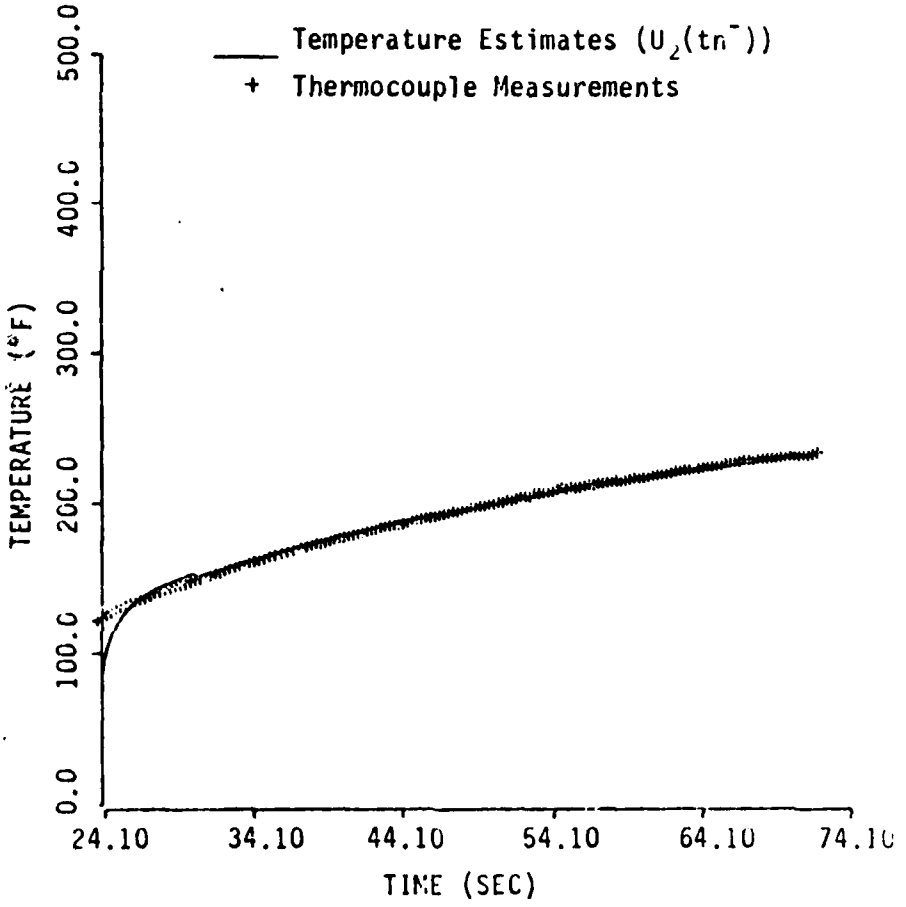

Figure D-10 Temperature Time History of Maneuver Three

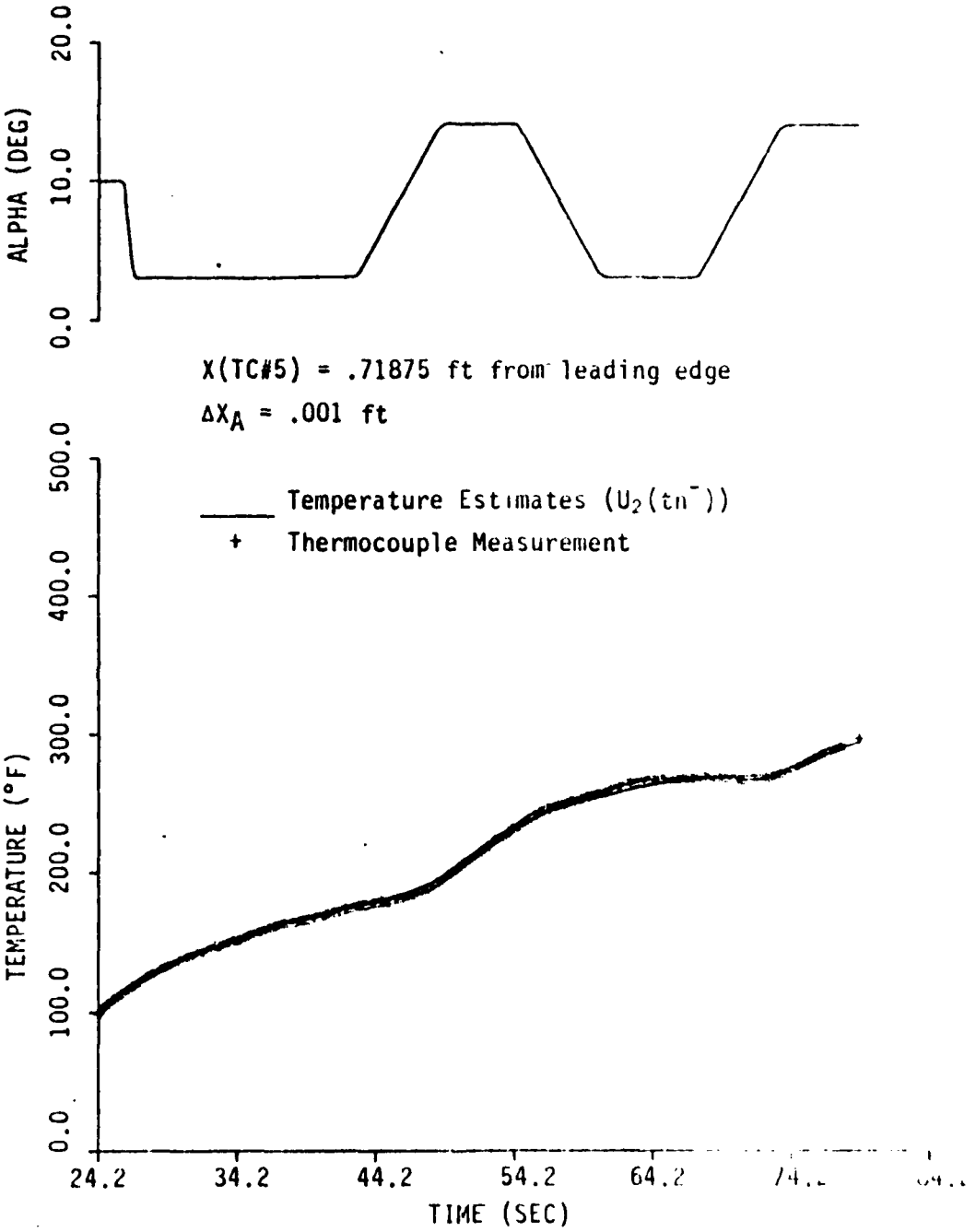

Figure D-11 Deflection Angle and Temperature Time History of Maneuver Four

HRSI SURFACE THERMOCOUPLE DATA

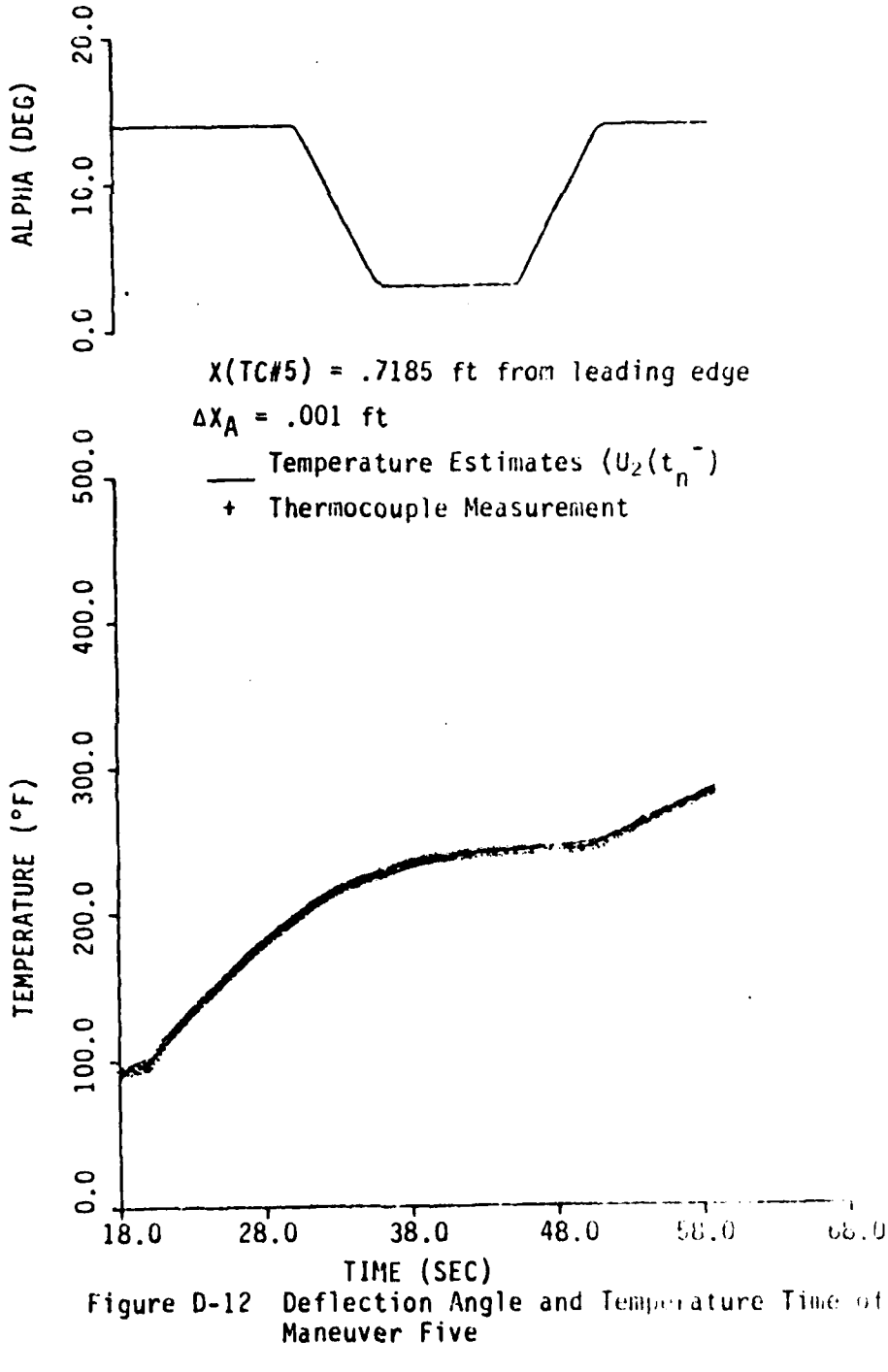

Figure D-12 Deflection Angle and Temperature Time of Maneuver Five

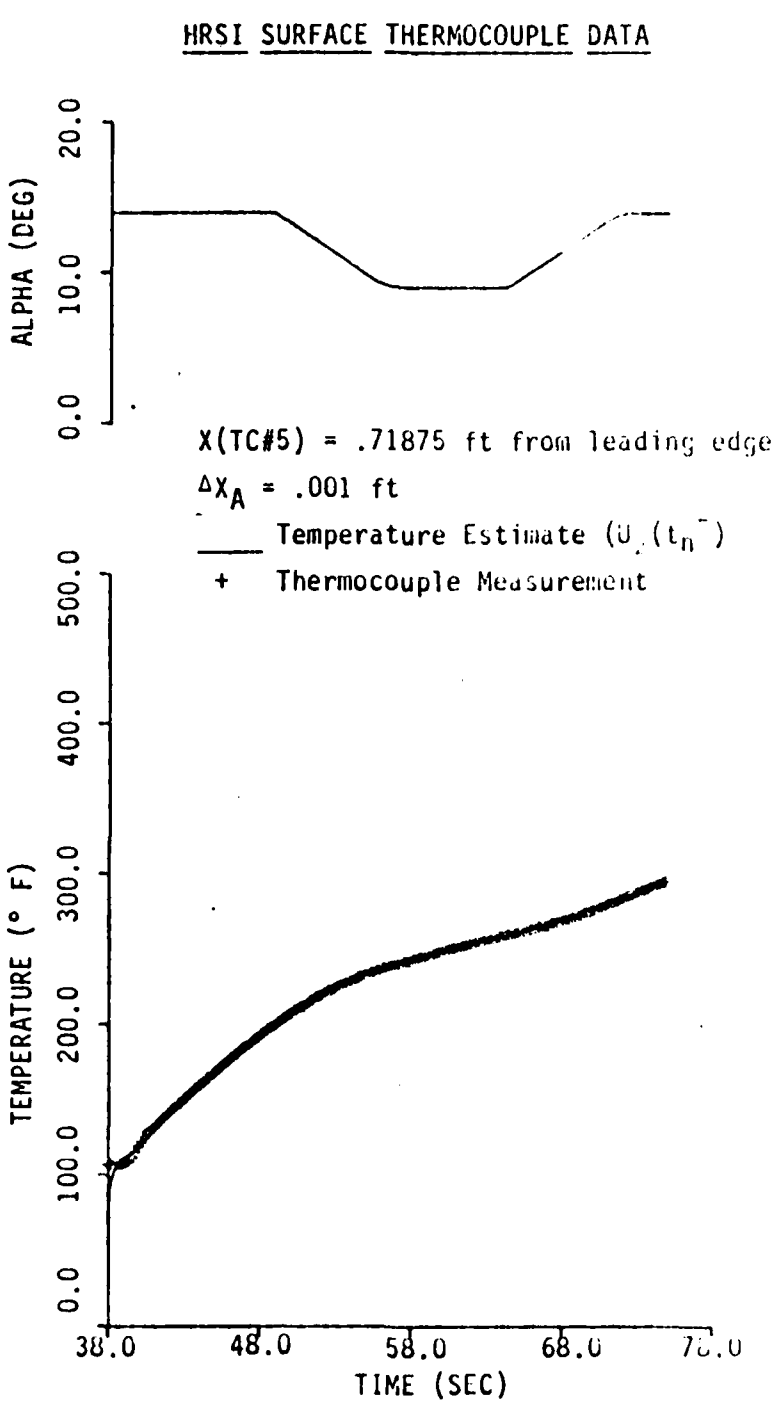

Figure D-13 Deflection Angle and Temperature Time History of Maneuver Six

HRSI SURFACE THERMOCOUPLE DATA

X(TC Location) = .71875 ft from leading edge

ΔX_A = .001 ft

$h_0/h_{ref}(\alpha_0 = 14°)$ = 2.28464

$h_\alpha/h_{ref}(\alpha_0 = 14°)$ = .10051

____ Temperature Estimates ($U_2(t_n^-)$)

\+ Thermocouple Measurement

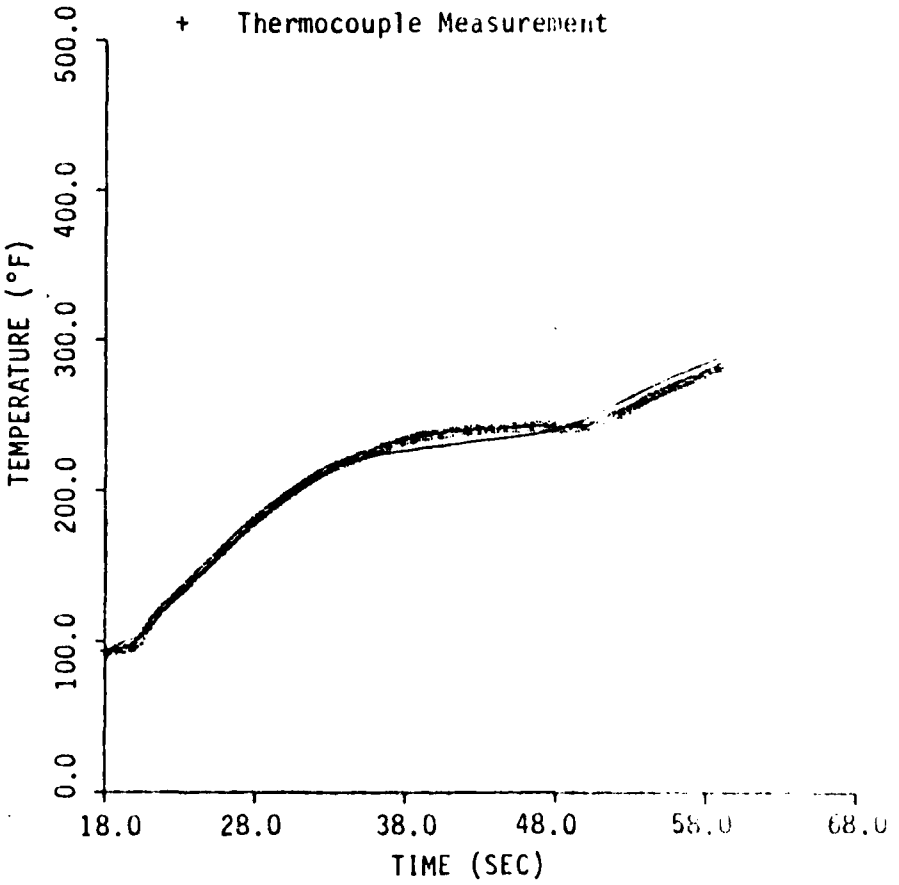

Figure D-14 Temperature Time History of Maneuver Five with Parameters Fixed Similar to a Simulator Run

HRSI SURFACE THERMOCOUPLE DATA

X(TC Location) = .71875 ft from leading edge

ΔX_A = .001 ft

$h_o/h_{ref}(\alpha_o = 14°)$ = 2.30388

$h/h_{ref}(\alpha_o = 14°)$ = .14215

____ Temperature Estimates ($U_i(t_n^-)$

\+ Thermocouple Measurement

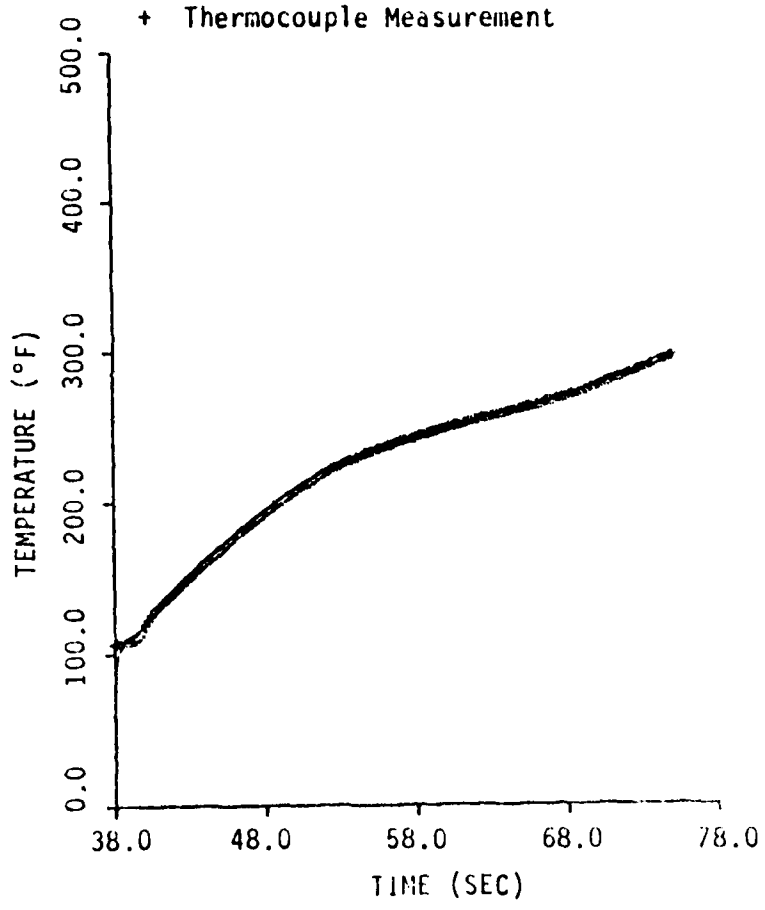

Figure D-15 Temperature Time History of Maneuver Six with Parameters Fixed Similar to a Simulator Run

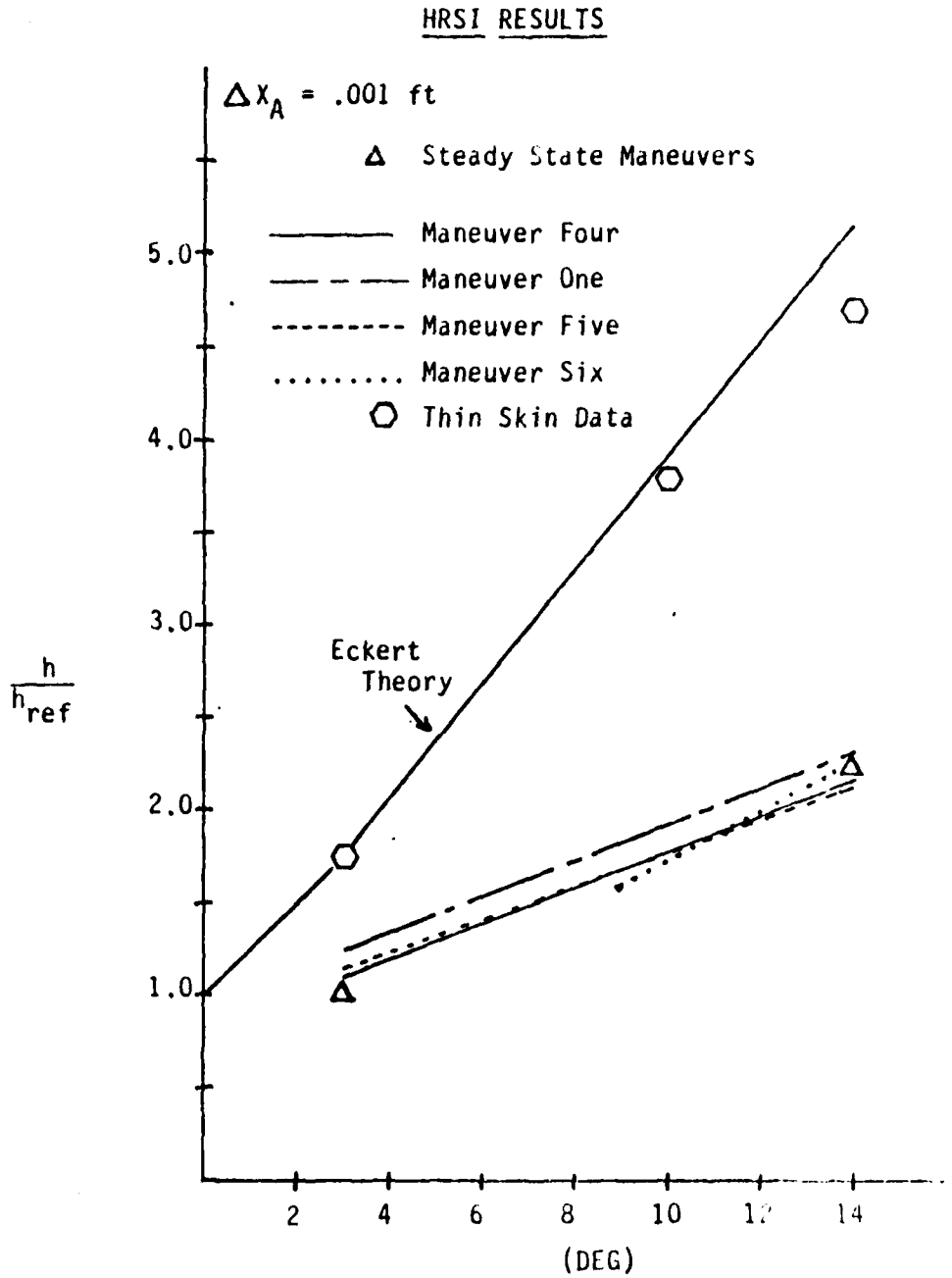

Figure D-16 Comparison of the HRSI, Thin Skin, and Eckert Theory Results

HRSI SURFACE THERMOCOUPLE DATA

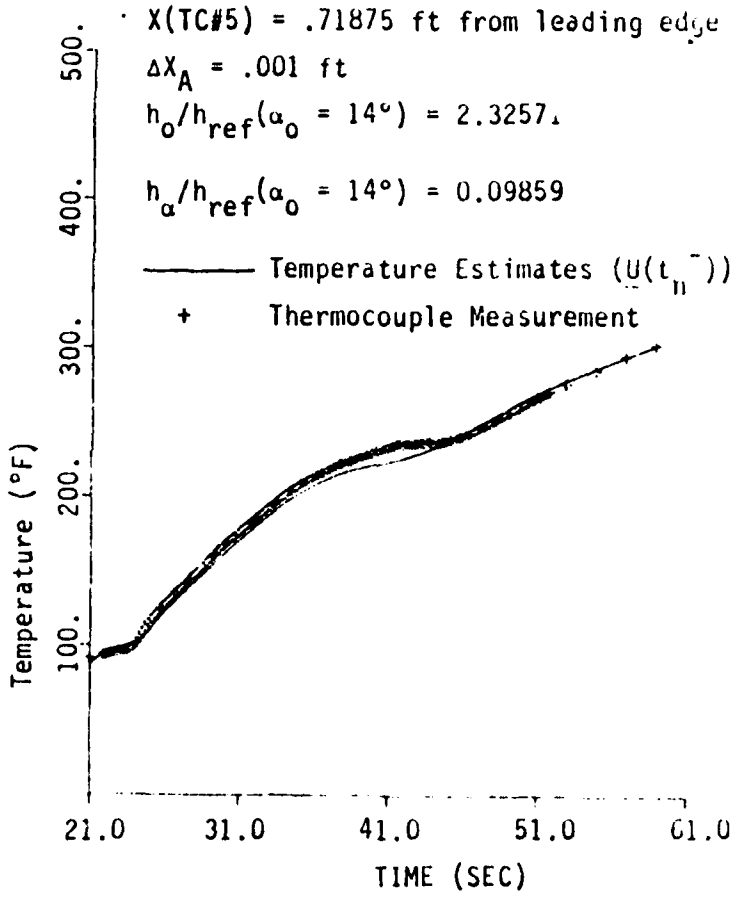

Figure D-17 Temperature Time History of Maneuver One with Parameters Fixed Similar to a Simulator Run Using the Heating Parameter Estimates from Figure D-16

FRSI SURFACE AND BONDLINE THERMOCOUPLE DATA

Constant Angle of Attack Equal to 14°

ΔX_A = .00058 ft

___ Temperature Estimates ($U_2(t_n^-)$)

\+ Thermocouple Measurement at Surface Node Number Two

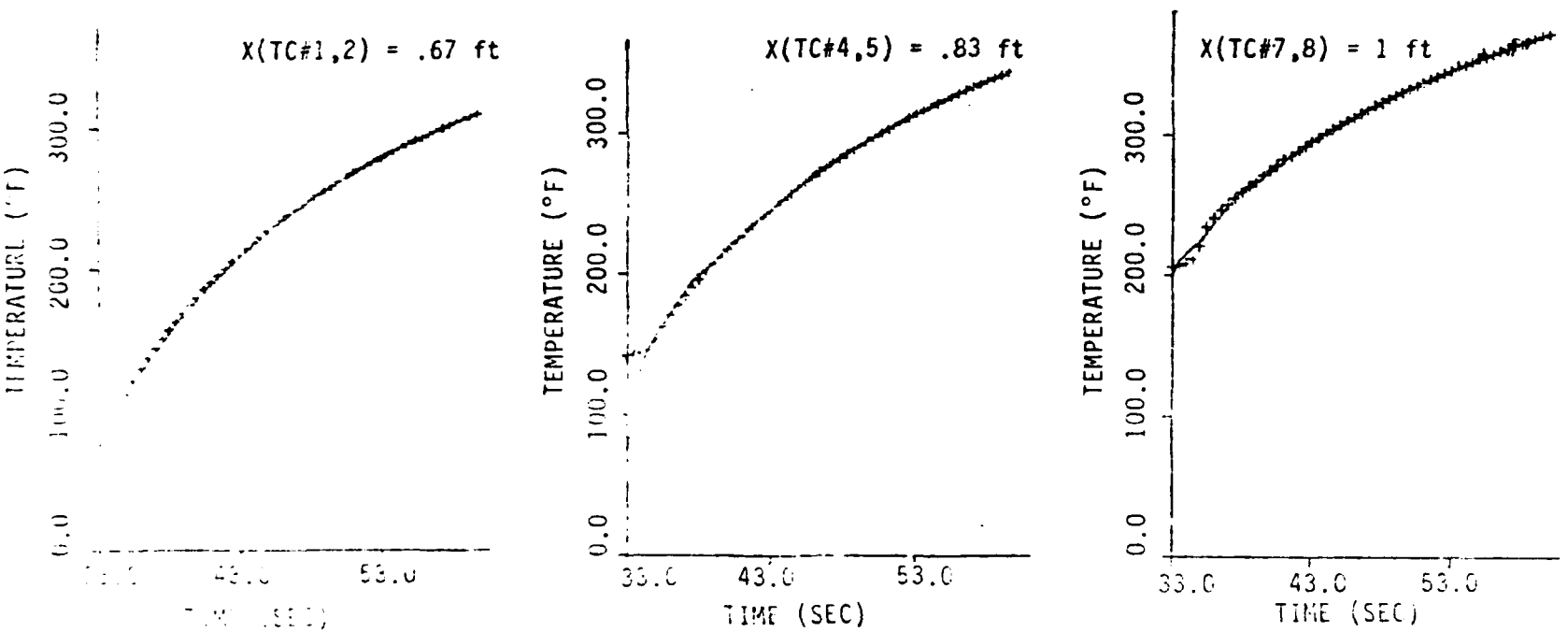

Figure [illegible] Temperature Time History of Maneuver Seven at Various Thermocouple Locations

FRSI SURFACE AND BONDLINE THERMOCOUPLE DATA

Constant Angle of Attack Equal to 3°

ΔX_A = .00058 ft

____ Temperature Estimates ($U_2(t_n^-)$)

\+ Thermocouple Measurement at Surface Node Number Two

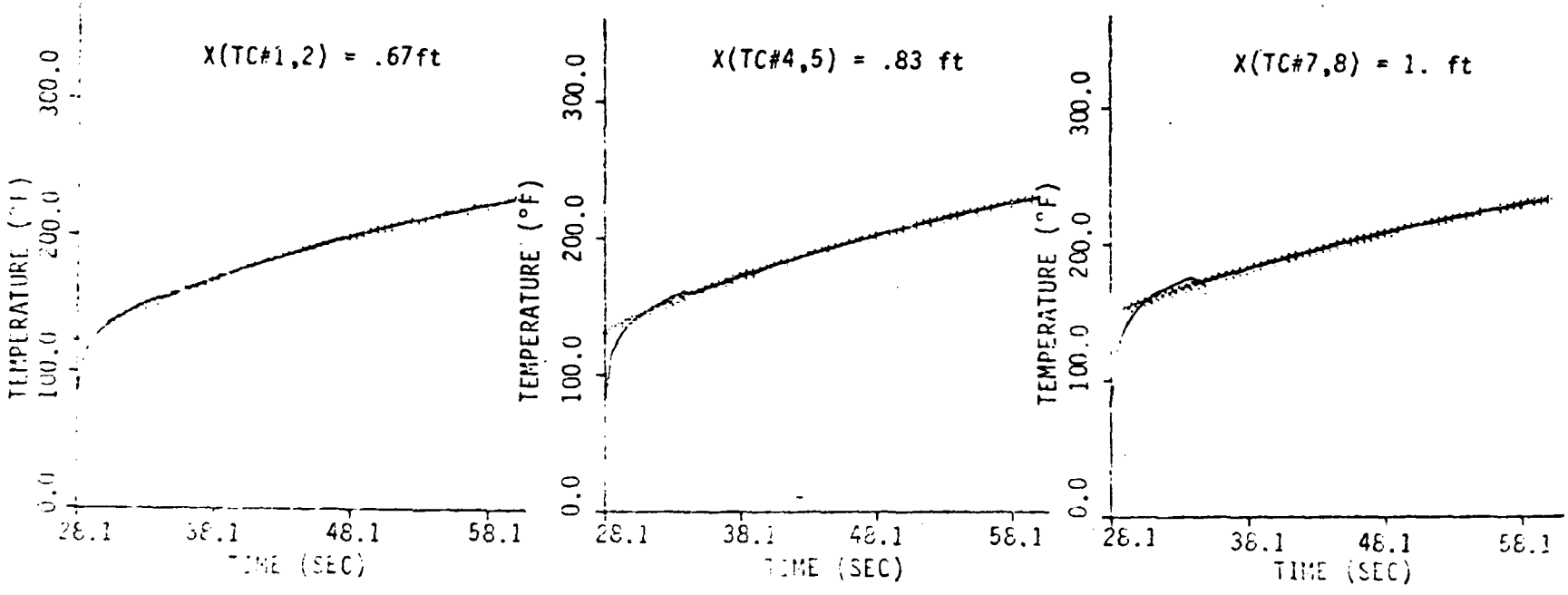

Figure 3-13. Temperature Time History of Maneuver Eight at Various TC Locations

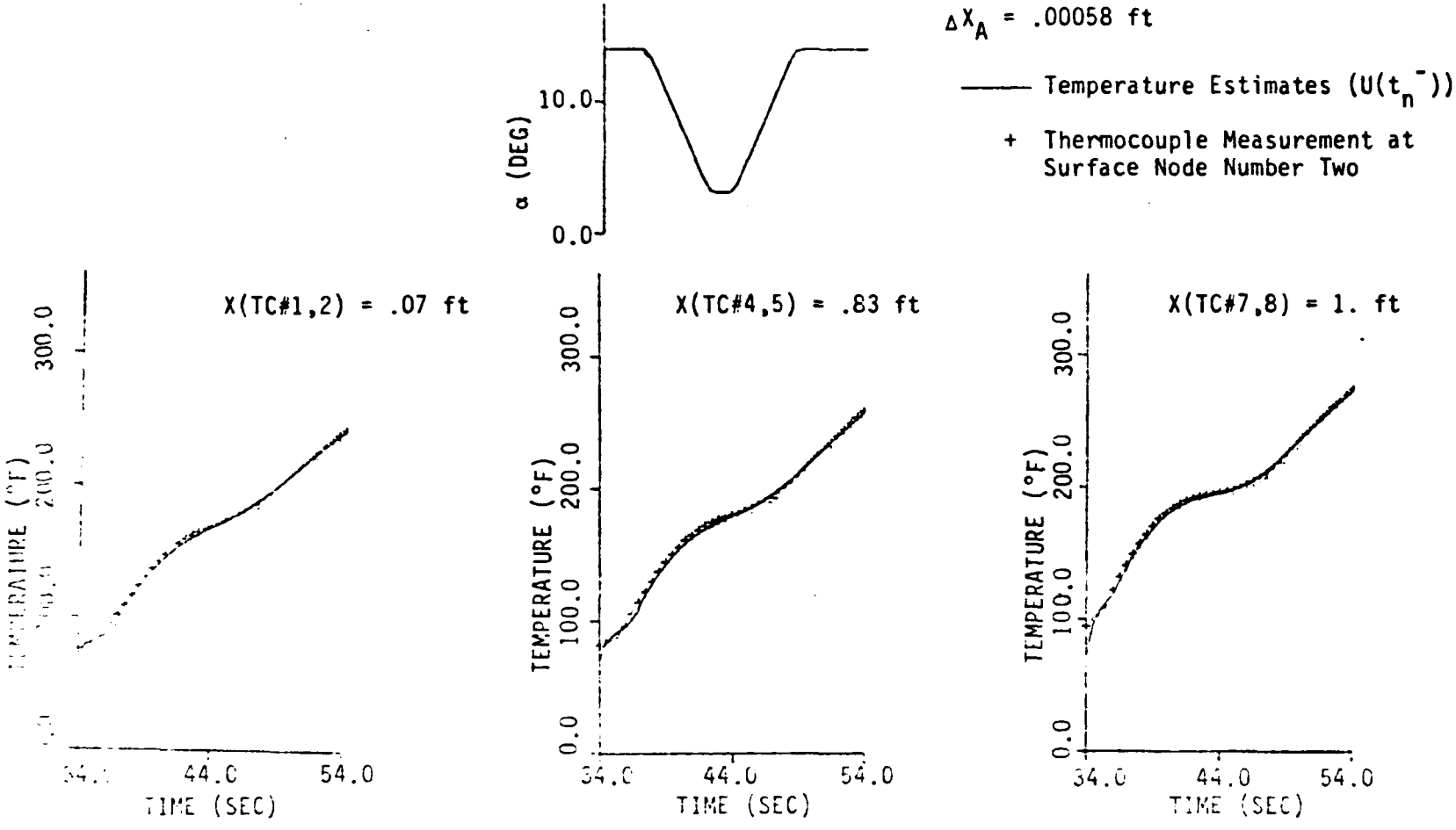

Figure D-23 Deflection Angle and Temperature Time History of Maneuver Nine at Various Thermocouple Locations

FRSI RESULTS

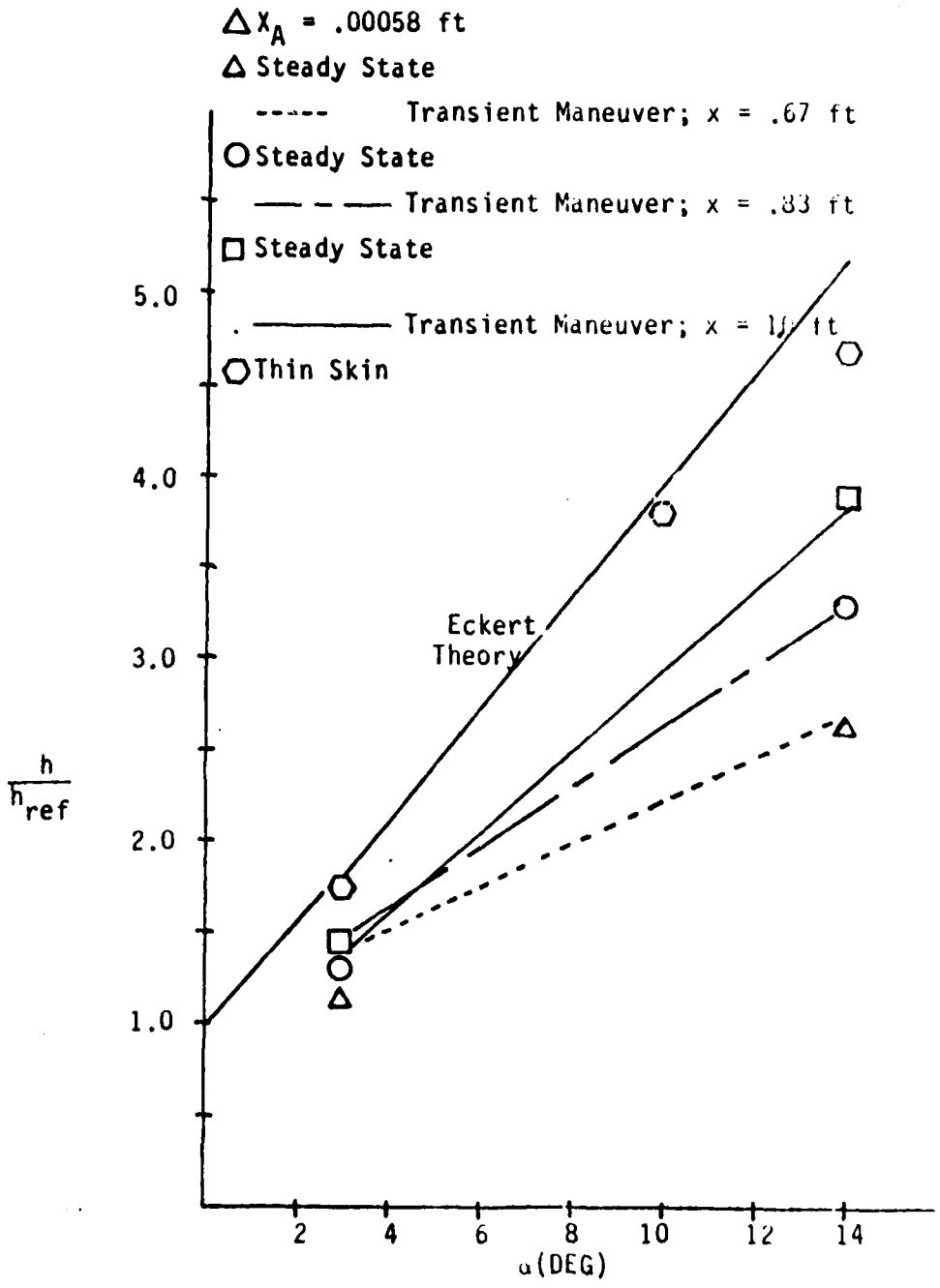

Figure D-21 Comparison of the FRSI, Thin Skin, and Eckert Theory Results

FRSI SURFACE AND BONDLINE THERMOCOUPLE DATA

ΔX_A = .00056 ft

____ Temperature Estimates (U (t_n^-)

\+ Thermocouple Measurement at Surface Node Number Two

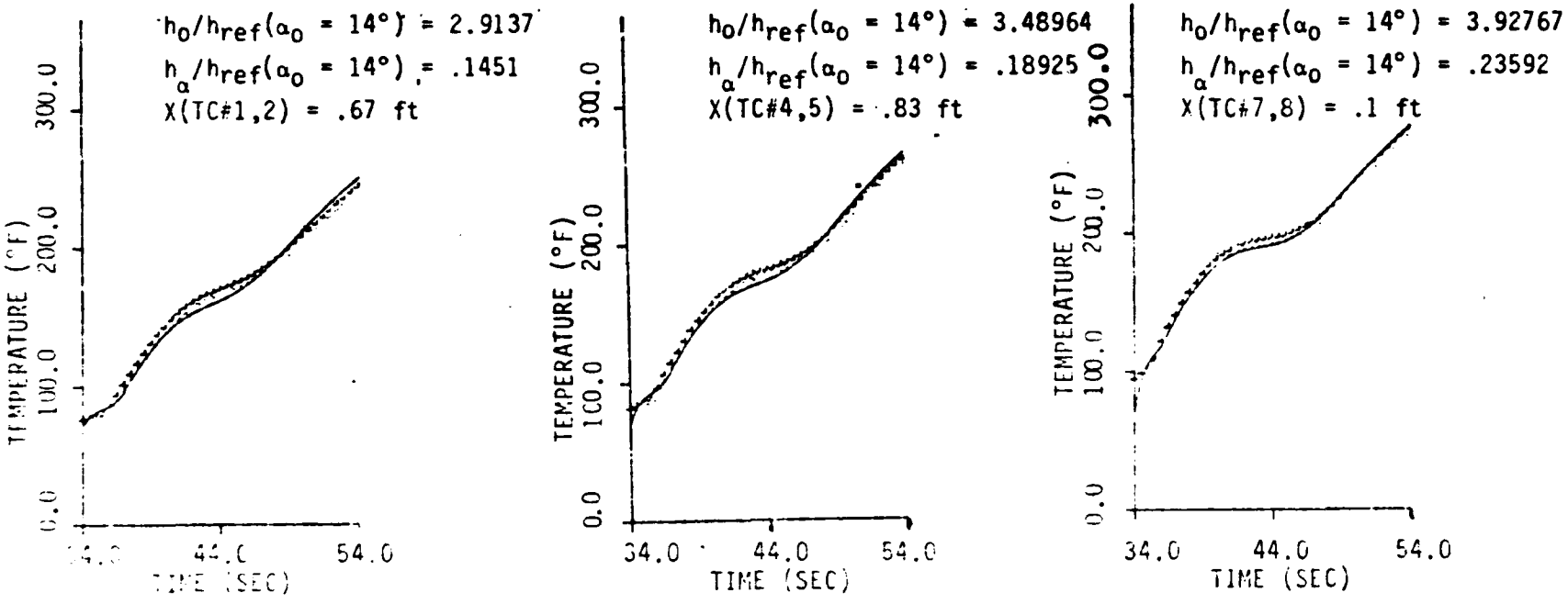

Figure D-11. Temperature Time History of Maneuver Mode with Parameters Fixed Similar to a Simulator Run at Various Thermocouple Locations

VITA

Yuk Kam Woo was born on 2 July 1958 in Hong Kong, the son of Ging Yow Woo and Ngan Fong Woo. He and his family immigrated to the United States in 1969. He graduated from Cleveland High School in Seattle, Washington in 1976. In August 1980, he was graduated with the degree of Bachelor of Science in Aeronautical and Astronautical Engineering at the University of Washington. He then entered the Officer Training School, and upon receiving his commission in the USAF, he entered the School of Engineering, Air Force Institute of Technology, in March 1981.

Permanent address: 7024 Covello Dr. So.
Seattle, Washington 98108

SECURITY CLASSIFICATION OF THIS PAGE *(When Data Entered)*

REPORT DOCUMENTATION PAGE	READ INSTRUCTIONS BEFORE COMPLETING FORM
1. REPORT NUMBER: AFIT/GAE/AA82D-34	2. GOVT ACCESSION NO.: AD-A124 163
	3. RECIPIENT'S CATALOG NUMBER
4. TITLE *(and Subtitle)*: TRANSIENT HEAT-TRANSFER MEASUREMENT TECHNIQUE IN WIND TUNNEL AND DATA ANALYSIS TECHNIQUE USING SYSTEM IDENTIFICATION THEORY	5. TYPE OF REPORT & PERIOD COVERED: MS Thesis
	6. PERFORMING ORG. REPORT NUMBER
7. AUTHOR(s): Yuk K. Woo	8. CONTRACT OR GRANT NUMBER(s)
9. PERFORMING ORGANIZATION NAME AND ADDRESS: Air Force Institute of Technology (AFIT-EN) Wright-Patterson AFB, Ohio 45433	10. PROGRAM ELEMENT, PROJECT, TASK AREA & WORK UNIT NUMBERS
11. CONTROLLING OFFICE NAME AND ADDRESS	12. REPORT DATE: December, 1982
	13. NUMBER OF PAGES: 90
14. MONITORING AGENCY NAME & ADDRESS *(if different from Controlling Office)*	15. SECURITY CLASS. *(of this report)*: Unclassified
	15a. DECLASSIFICATION/DOWNGRADING SCHEDULE

16. DISTRIBUTION STATEMENT *(of this Report)*

Approved for public release; distribution unlimited

17. DISTRIBUTION STATEMENT *(of the abstract entered in Block 20, if different from Report)*

18. SUPPLEMENTARY NOTES

Approved for public release: IAW AFR 190-17.
LYNN E. WOLAVER
Dean for Research and Professional Development
Air Force Institute of Technology (AIC)
Wright-Patterson AFB OH 45433
19 JAN 1983

19. KEY WORDS *(Continue on reverse side if necessary and identify by block number)*

Heat Transfer
Thermocouple
Space Shuttle Thermal Protection System
Kalman Filter
System Identification Theory

20. ABSTRACT *(Continue on reverse side if necessary and identify by block number)*

A transient maneuver testing technique has been developed by the Air Force Flight Test Center (AFFTC) for aerothermodynamic evaluation of the Space Shuttle Orbiter Thermal Protection System (TPS) during reentry. The objectives are to determine the feasibility of the testing technique and the feasibility of using the transient maneuver technique for wind tunnel heat transfer measurements. The transient maneuver technique can enhance the capability of wind tunnel testing by reducing the overall required testing time, and in turn lower the cost

DD FORM 1 JAN 73 1473 EDITION OF 1 NOV 65 IS OBSOLETE

SECURITY CLASSIFICATION OF THIS PAGE *(When Data Entered)*

of testing significantly.

Wind tunnel data were obtained using the TPS materials of the Orbiter as wind tunnel test articles. Transient and steady state deflection angle data were obtained and analyzed. The thermocouple measurements along with the wind tunnel conditions were used as inputs to a heat estimation computer program. The program named "HEATEST" was developed by AFFTC and used system identification theory. The results of the estimates were compared with the available thin skin data and also with the Eckert flat plate theory.

The principle finding indicates the heating estimates are significantly lower for the TPS test articles than the thin skin test article and Eckert theory. The discrepancy is believed to be caused mainly by the non-isothermal wall effect. Finally, the transient maneuver testing technique has been proven since the transient maneuvers agree well with the steady state results.

END

FILMED

3-83

DTIC